ARL 67-0071

CONDENSATION IN A RAPIDLY EXPANDING METAL VAPOR-INERT GAS MIXTURE

P. M. SHERMAN
D. D. McBRIDE
E. OKTAY

THE UNIVERSITY OF MICHIGAN
DEPARTMENT OF AEROSPACE ENGINEERING
ANN ARBOR, MICHIGAN

APRIL 1967

Contract No. AF 33(615)-2307
Project No. 7116

AEROSPACE RESEARCH LABORATORIES
OFFICE OF AEROSPACE RESEARCH
UNITED STATES AIR FORCE
WRIGHT-PATTERSON AIR FORCE BASE, OHIO

FOREWORD

This Interim Technical Report was prepared on work done under Contract AF-33(615)-2307 between Aerospace Research Laboratory, Office of Aerospace Research, United States Air Force and The University of Michigan. It was first under the technical cognizance of Mr. E. Stephens of the Thermo-Mechanics Research Laboratory of ARL and then under the technical cognizance of Mr. S. Hasinger of the Energetics Research Laboratory, ARL.

ABSTRACT

An investigation of the condensation of metal vapor in an inert carrier gas accelerated through nozzles is being carried out. The mixture used is primarily zinc vapor in helium gas. The zinc vapor is produced in two separate experimental arrangements. One is in the arc chamber of an inductance type hot shot tunnel. The other is in an exploding-wire chamber with a capacitor energy storage. Two types of condensation measurements are made. Measurement of particle size is made in the tunnel. Determination of condensation onset point is made in the exploding-wire system. Particle size is determined by means of a shuttered sampling device developed for the purpose combined with electron microscope techniques evolved. The condensation onset point is determined by nozzle static pressure measurement. Simplified computational analyses are made to predict conditions for the measured condensation onset point. They are also used as a guide for the more complex two component non-equilibrium expansion computation which may predict the location of the onset point as well as particle size. Measurements of particle size at the exit of a nominal Mach 25 (helium) nozzle showed a major portion of the total particles to be less than ~ 70 Å in diameter. The pressure measurements made in a nominal Mach 3 nozzle indicated a large degree of supercooling. Further studies and evaluations to be made are discussed.

TABLE OF CONTENTS

LIST OF ILLUSTRATIONS

Introduction

The study of condensation phenomena has become of special interest in recent years as a result of problems arising in modern applications in gas dynamics. The operation of wind tunnels is limited by condensation which occurs as the gas is expanded to higher velocities with the corresponding very low temperatures. The performance of turbines, especially those employing metal vapors, is determined in large extent on condensation. Condensation has been investigated for the production of colloidal particles for electric propulsion devices. When metal additives are used in rocket engines, condensation of metal oxides has a strong influence on the combustion rate and thrust generated. These and other applications require a greater ability to predict conditions for condensation than is now possible.

The prediction of such aspects of condensation as size of particles generated, rate of growth, and degree of supersaturation under given conditions of temperature, pressure, rate of expansion, etc., have become important. In most cases of interest the departure from saturation equilibrium conditions can be very large. Results of both theory and measurement have been inadequate for predicting the extent of such departure from equilibrium as well as other condensation parameters. References (1) and (2) have a good summary of the earlier condensation work done. They include the simplified macroscopic or classical theories of nucleation and growth, and simplified one-dimensional

Manuscript released March 1967.

flowing vapor equations as well as a discussion of experimental techniques and experimental results. Reference (3) is a symposium on some of the later condensation work including microscopic aspects of the problem.

The present program is directed toward obtaining data which will permit the prediction of condensation parameters. In particular, measurements which will enable the prediction of particle size and degree of supercooling as a function of expansion rate and level of temperature, pressure and concentration, are of interest. The condensation of metal vapor in an inert carrier gas is of special interest here.

Production of Metal Vapor

One problem which arises in the study of condensation of metal vapor, is the production of the extreme conditions necessary to obtain metal at the appropriate temperature and pressure. Two methods have been used to obtain the superheated metal vapor. One makes use of an inductance type hot-shot tunnel. The other employs an exploding wire arrangement. The present experiments in both facilities have been primarily with zinc vapor in helium as a carrier gas.

The hot-shot tunnel is a blow-down type of facility described in Ref. (4). It makes use of energy initially taken from a 150 HP motor stored over a "long" period of time as kinetic energy of a heavy flywheel. The stored energy is transferred to the magnetic field of a large coil by means of a unipolar generator designed to deliver high current at low voltage. The energy

is discharged through an arc across electrodes inside the high pressure stagnation chamber. The arc is initiated by means of a fuse-switch arrangement which was redesigned (Ref. 5) so that the desired amount of zinc vapor would be obtained during the arcing process. Conditions are chosen so that the metal vapor is superheated and a baffle arrangement prevents particles from exhausting out of the stagnation chamber. Figure 1 shows a schematic of the arc-chamber-nozzle arrangement.

The tunnel stagnation chamber is initially charged with the desired amount of carrier gas (helium) so that when arcing occurs the transfer of energy raises the temperature and pressure of the mixture at constant volume. The resulting high temperature, high pressure gas mixture then consists of a hot carrier gas plus superheated metal vapor. The metal vapor-carrier gas mixture then may be expanded through an appropriate nozzle into the evacuated receiver tank.

The exploding wire arrangement is described in Appendices A and B. Energy is stored in capacitors and discharged through a small wire chosen for "optimum" (see Appendix A) conditions. The wire is mounted inside a pressure chamber which is initially charged with the desired amount of helium. The wire evaporates very rapidly increasing temperature and pressure of the mixture of carrier gas and metal vapor in the chamber. The hot high pressure mixture is expanded through an appropriate nozzle to atmosphere. This arrangement operates essentially as a small blow-down wind tunnel. Figure 2 shows the stagnation chamber-nozzle arrangement.

Operating Conditions in the Tunnel

Measurements were made primarily with zinc in helium. A nominal Mach 25 (helium) nozzle was used in the tunnel with a free-jet arrangement. The nozzle has an exit diameter of ~ 3 1/4 in. and exhausts into an evacuated ~ 20 in. diameter test section and large (4 ft diameter) vacuum tank. Stagnation pressures used were up to ~ 5000 psia with stagnation temperatures to ~ 5000^{o}K. The mass fraction of zinc was up to a maximum of ~ .7.

Stagnation temperatures are calculated from the measured stagnation pressure, assuming an ideal gas mixture and the known mass of helium and measured mass of zinc lost from fuse-switch and electrodes. This calculated temperature is within about 10% of the stagnation temperature calculated from the measured stagnation pressure but assuming zinc-free pure helium. That is, the mass of zinc required to saturate the mixture is three to five times higher than the mass of zinc vaporized in the arc chamber. The metal vapor therefore, starts out by being highly superheated.

Operating Conditions in the Exploding Wire Arrangement

Although some measurements were made with other metals (copper and iron) and carrier gases (nitrogen and argon) zinc in helium was primarily the mixture used. A nominal Mach 3 nozzle with exit diameter ~ 1/8 in. exhausting to the atmosphere was employed with this system to date. Measurements were made at stagnation pressures up to ~ 1000 psia at stagnation temperatures up to ~ 2500^{o}K in a stagnation chamber ~ 15.3 in.^{3} The zinc

wire used was 2.8 in. long and varied in diameter from .0403 to .0445 in. depending on the conditions desired. The mass fraction of zinc was varied from ~ .46 to ~ .765. The energy stored at 17.5 KV was 4500 joules, enough to leave the zinc vapor in a much superheated state. The efficiency of the energy transferred was ~ 60% to 75% for the "optimum discharge" (Appendix A) conditions and ~ 35% to 70% at other times. It should be noted that efficiency goes up with increase in stagnation chamber charge pressure and the efficiencies below 50% were at lower charge pressures than those used with the "optimum discharge" conditions. The efficiency was determined by comparing the energy stored in the capacitors and the energy computed from the measured stagnation pressure. (See Appendix E.)

Measurements - General

Figure 3 is a photograph of a tunnel run record made of current, voltage and pressure measurements as a function of time. It also shows the timing and sequencing of shutter and valves. The traces shown were recorded on a CEC (Consolidated Engineering Corporation) Recording Oscillograph Model S-119. The top trace represents the 24 volt source which energizes the solenoid used to control the main power transfer switch. The second trace is the output of a Hall effect current transducer located on the arc chamber axial bussbar upright connectors and measures the current through the electrodes. The next two traces are the outputs of two Ultradyne 0.1 PSID variable reluctance pressure transducers energized by 20KC carrier amplifiers. The

first of these shows static pressure in the interior of the sampler housing and the second measures the ambient receiver pressure at the front of the receiver tank. The pitot probe at the exit of the nozzle is located on the centerline 1/4 in. from the sampler inlet slit. A 30 PSID Hidyne variable reluctance pressure transducer energized by a 20KC carrier amplifier is used to measure this pressure. The trace of the output of the (Electromation Model 3030) magnetic pickup indicates one "blip" to represent one revolution of the collector cylinder. The stagnation pressure is measured by a Baldwin-Lima-Hamilton 10,000 PSIG Type GP strain gage pressure transducer energized by a 20 KC carrier amplifier. Gates A and B represent the gate outputs of the oscilloscope used to trigger the shutter solenoid and the magnetic valve (see Appendix C). The voltaic cell trace locates the sampling point (see Appendix C). The arc voltage is obtained from a small coil placed inside the hot-shot main energy storage coil so that the collapsing magnetic field produces a current in the pickup coil proportional to the arc voltage. The last trace simply indicates the point of dump valve actuation.

Exploding wire current and voltage traces were recorded as described in Appendix A. Figure 4 is a reproduction of pressure traces recorded in the exploding wire system. A description of measurement and recording methods appear in Appendix B.

Measurements - Condensation

Primarily two types of condensation measurements were made. Measurements in the tunnel have been of particle size and measurements in the exploding wire system have been of the condensation onset point. The present plan is to combine the two types of measurements, and make them simultaneous. The determination of particle size is being accomplished using an electron microscope with sampling techniques. The condensation onset point is being determined by static pressure measurements.

The problems involved in sampling are many. The primary one, of course, is to accomplish the sampling without disturbing the flow or specimen. Any probe must somehow decelerate a section of stream in such a way that the flow field and sample remain unchanged or in such a way that all changes can be accounted for. A wedge shaped "skimmer" with a very narrow slit at the leading edge but with pressure inside matched to ambient should produce a narrow free jet downstream inside the sampler. As the free jet issues into the surrounding gas it is then decelerated gradually by viscous mixing. If the jet is very narrow the temperature then remains low enough to prevent reevaporation before collection. This idea was used in the development of samplers described in Appendix C. Two types of samplers are described, one with a rotating shutter and one with a sliding shutter (Figs. C-2, C-4). The rotating shutter was designed to permit several collections in time with space resolution. The linear shutter permits only one collection at a given time and only

over 1/4 in. of length. In both cases the flow at the exit of the nozzle passes through a very narrow slit (~ .01 in. wide) at the leading edge of a wedge and into a chamber with pressure matched to nozzle exit pressure. The very narrow (see Appendix C) sampled "jet" is then slowed down by viscous mixing in the sampler. The condensed particles impinge on a rotating cylinder which is covered with strips of mica, coated with ~ 160 Å thick carbon layer.

After the particles are collected the strip of mica is shadowed with chromium to show three-dimensional effects. Sections of the specimen are then cut out. The carbon film with particles and chromium layer is floated off the mica on water and mounted on an electron microscope grid. Sections of the grid are then photographed under the electron microscope. Figure 5 shows such a photograph. The sampling was done at the exit of the Mach 25 nozzle. Conditions in this case were such that all the condensible vapor would be expected to be condensed out far upstream of the nozzle exit.

Appendix C has a description of the techniques used in obtaining and photomicrographing particles.

When condensation occurs in a supersonic nozzle, the resulting heat addition to the stream increases the static pressure. During a rapid expansion the stream tends to become supercooled so that when condensation occurs it occurs rapidly. The point at which condensation begins (condensation onset) can then be detected by a jump in nozzle pressure. This method of detecting condensation onset is being used in the exploding wire system. The stagnation

temperature and pressure in the exploding wire chamber (Fig. 2) decreases with time as the metal vapor carrier gas mixture blows out through the nozzle. If stagnation conditions are such that initially the condensation onset point is downstream of the exit of the nozzle, then as the system blows down the onset point will tend to move upstream with time. A trace of pressure as a function of time at a given location should then be similar to a trace of pressure as a function of distance along the nozzle for the case of stagnation conditions constant in time. Figure 4 shows a reproduction of three such traces where as the initial stagnation temperature is reduced from 2210^{o}K to 1790^{o}K, a pressure increase "bump" appears and is located at an earlier time as the stagnation temperature is decreased. The initial stagnation pressure in these traces vary from 685 to 755 psia.

To take the greatest advantage of the pressure change indication of condensation a new nozzle section was made with pressure mountings spaced all along its length (Fig. 6). In this way simultaneous pressures may be obtained at each station and pressure as a function of location at a given time, as well as pressure as a function of time at a given location may both be obtained. The sampling techniques and pressure measurements then will be simultaneously employed with this nozzle.

Computational Analysis

The classical liquid drop theory of condensation is the one most widely used to obtain homogeneous nucleation rates for non-equilibrium condensation. Unfortunately the theory depends radically on the value of surface

tension (Ref. 6) used. These values are generally not well known, especially for particles of very small radius. Although the theory has been questioned to a large extent on several counts (see symposium of Ref. 3), it provides a guide for prediction of some condensation parameters.

A computer study of condensation in expanding one component flows was completed as a separate report (Ref. 7). Effects of rate of expansion, and variations in pressure, temperature and entropy levels were considered. Heterogeneous effects were also treated.

A program for the non-equilibrium condensation of the two component mixture of a vapor in an inert carrier gas was initiated but has not as yet been working. As a result, two simpler sets of calculations were made as guides for the experimental work and the more complex calculations. One is the equilibrium condensation solution. The other is the "condensation shock" solution. (Both of these analyses are described in Appendix D.) The "condensation shock" solution assumes that at each or any point in the nozzle, the condensation takes place instantaneously (as a discontinuity) from "frozen" to saturation conditions. A locus of such points can then be determined. Each point on the locus then represents the conditions downstream of a different condensation discontinuity. The equilibrium solution assumes isentropic flow to the point where the vapor pressure curve is intersected and then saturation conditions downstream of that point. The equilibrium solution represents conditions at each point in a given nozzle for given stagnation conditions when no supercooling occurs.

The "condensation shock" solution yields a higher pressure and a lower mass of condensate than the saturated equilibrium solution. The percentage increase in pressure difference between the two solutions increases with the degree of supersaturation which exists before the "shock" occurs. The actual non-equilibrium expansion would be expected to approach equilibrium from a supersaturated state very rapidly but not instantaneously or discontinuously. That is, the approach to equilibrium occurs over a finite region, the extent of which depends on the rate of expansion and the initial departure from equilibrium. The locus of "condensation shock" solutions predicts the maximum possible increase in pressure as a result of condensation in the nozzle. The expected nozzle pressure however, for conditions considered here, would probably show a rapid approach at the condensation onset from "frozen" isentropic conditions to only slightly above that given by the saturated equilibrium solution.

Figure 7 shows a comparison of "frozen" isentropic (supercooled, no condensation) nozzle pressure with the saturated equilibrium expansion nozzle pressure for two initial mass fractions of condensible vapor. The initial conditions are those typical for a zinc in helium tunnel run. The nozzle is the nominal Mach 5 nozzle (Fig. 6). As the mass fraction of zinc increases, the point at which the equilibrium saturation curve departs from the isentropic curve, (where either condensation or supersaturation must occur) moves downstream. The amount of condensate and pressure difference then depends on

distance from that point. Figure 8 shows a similar solution for the nominal Mach 25 nozzle. Figure D-1 shows a comparison of the "condensation shock" solution with the saturated equilibrium solution for the nominal Mach 3 nozzle.

Discussion of Results and Continued Investigations

Present tests indicate that measurements of particle size are feasible using the dynamic sampling techniques developed with the electron microscope techniques evolved. Figure 9 shows particle size distribution determined from photomicrographs of samples taken at the exit plane of the Mach 25 nozzle, where it would be expected that all of the zinc had condensed out long before reaching the exit of the nozzle. The different symbols in the figure represent different magnifications used. Low magnification photographs are used to count large particles and high magnification for the small particles. The count is then normalized by the width of diameter increment measured. As the figure indicates, the number of particles in the range between 50 $\mathring{A}$ and 70 $\mathring{A}$ in diameter is very much greater than the number of larger particles. (Note logarithmic coordinates, the larger particles could not be seen on a linear plot.) Examination of photomicrographs such as Fig. 5, however, shows that the grain size of the chromium layer is such that particles smaller than ~ 40 $\mathring{A}$ could not be detected. It is possible that by using platinum instead of chromium with a somewhat different shadowing technique, the grain size may be reduced. Photomicrographs of samples taken from wall surfaces inside the sampler showed a negligible number of particles are not "caught" by the rotating

cylinder collecting surface—unless the particles are smaller than 40 Å. The latter possibility will be checked with different electron-microscope techniques.

Although the metal vapor-helium mixture is initially superheated and a baffle is employed to separate any particles from the flow, it appears advisable to make doubly sure that the particles collected are not from the stagnation chamber. The present idea is to add a baffled settling chamber such that any small particles from the stagnation chamber would evaporate, large particles would be baffled out and, in addition, the mixture would be further superheated by the shock reduction in stagnation pressure. That is, the metal vapor would be at a lower pressure at similar total temperature to that in the stagnation chamber.

The calculations made indicate that condensation onset may be observed as a large increase in nozzle static pressure (see Figs. 7, 8, D-1). Of course, the increase in pressure is a function of mass fraction of condensate as well as the stagnation entropy which determines where the saturation conditions are reached. Figure 4 shows the result of some nozzle pressure measurements made near the exit of the Mach 3 nozzle. Figure 4(a) indicates no condensation during the period of blowdown. Figure 4(b), for a lower initial stagnation temperature, shows the onset of condensation, and Fig. 4(c) for an even lower initial stagnation temperature shows condensation onset occurring sooner. (The pressure reference lines shown are atmospheric pressure, not zero pressure.)

It is reasonable to assume that long before the condensation onset point, the trace represents an isentropic expansion and long after the onset, the trace represents saturated equilibrium. If the part of the trace before the onset "bump" is taken as the isentropic expansion the boundary layer displacement thickness just before the onset point can be determined. In addition, if long after the "bump" it is assumed that saturation conditions are reached, then the mass fraction of zinc can be determined. When this is done, the mass fraction of zinc obtained appears to be much less than that based on the zinc vaporized in the stagnation chamber. However, even with the smaller mass fraction, a large degree of supersaturation or departure from equilibrium is indicated. This is consistent with a "bump" in the pressure trace. For quantitative results a better determination of mass fraction of zinc is to be made.

As temperature in the stagnation chamber decreases at a given pressure, saturation conditions are reached further upstream in the nozzle. A saturated equilibrium expansion for different stagnation temperatures but constant mass fraction would then appear similar to those for different mass fractions at constant stagnation temperature. That is, a decrease in stagnation temperature at a given stagnation pressure may look like an increase in mass fraction. During a run only a fraction of the gas mixture in the stagnation chamber blows out. This means that if temperature or zinc vapor concentration gradients exist in the stagnation chamber then the effective stagnation

temperature and zinc mass fraction for the nozzle flow could be different from that determined from measured stagnation pressure, assuming equilibrium conditions in the stagnation chamber. Further computations to investigate these possibilities and the settling chamber mentioned earlier to eliminate such gradients, is being initiated.

A check on the boundary layer displacement thickness downstream of the condensation zone and the mass fraction of zinc could be accomplished by making use of a method employed by Thomann (Ref. 8).. It is shown in Ref. 8 that by using pitot tubes of different diameters, when a large enough diameter is reached a further increase in diameter makes no difference in the measurement—or a "correct" number of free stream particles must then be evaporated. This measurement combined with the stagnation chamber pressure measurement yields an effective displacement thickness which may be compared with the one determined earlier. In addition, combining the nozzle static pressure measurement with the possible other limit of pitot tube size where there is no time for reevaporation, may yield an added check.

The simultaneous combination of condensation onset measurements with particle size determination should yield information on particle growth rate as well as the degree of departure from equilibrium to be expected.

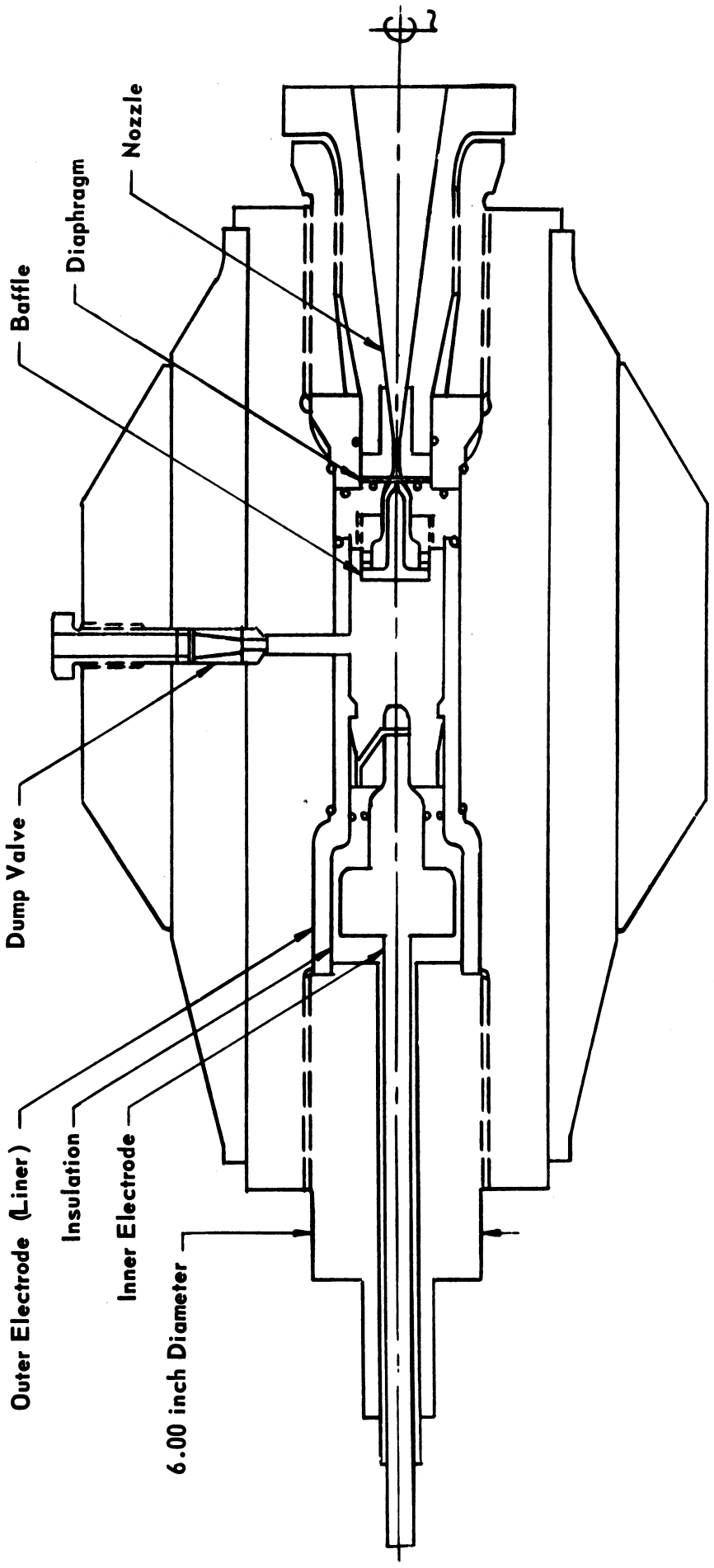

Figure 1. Sketch of the Hotshot Arc Chamber Assembly

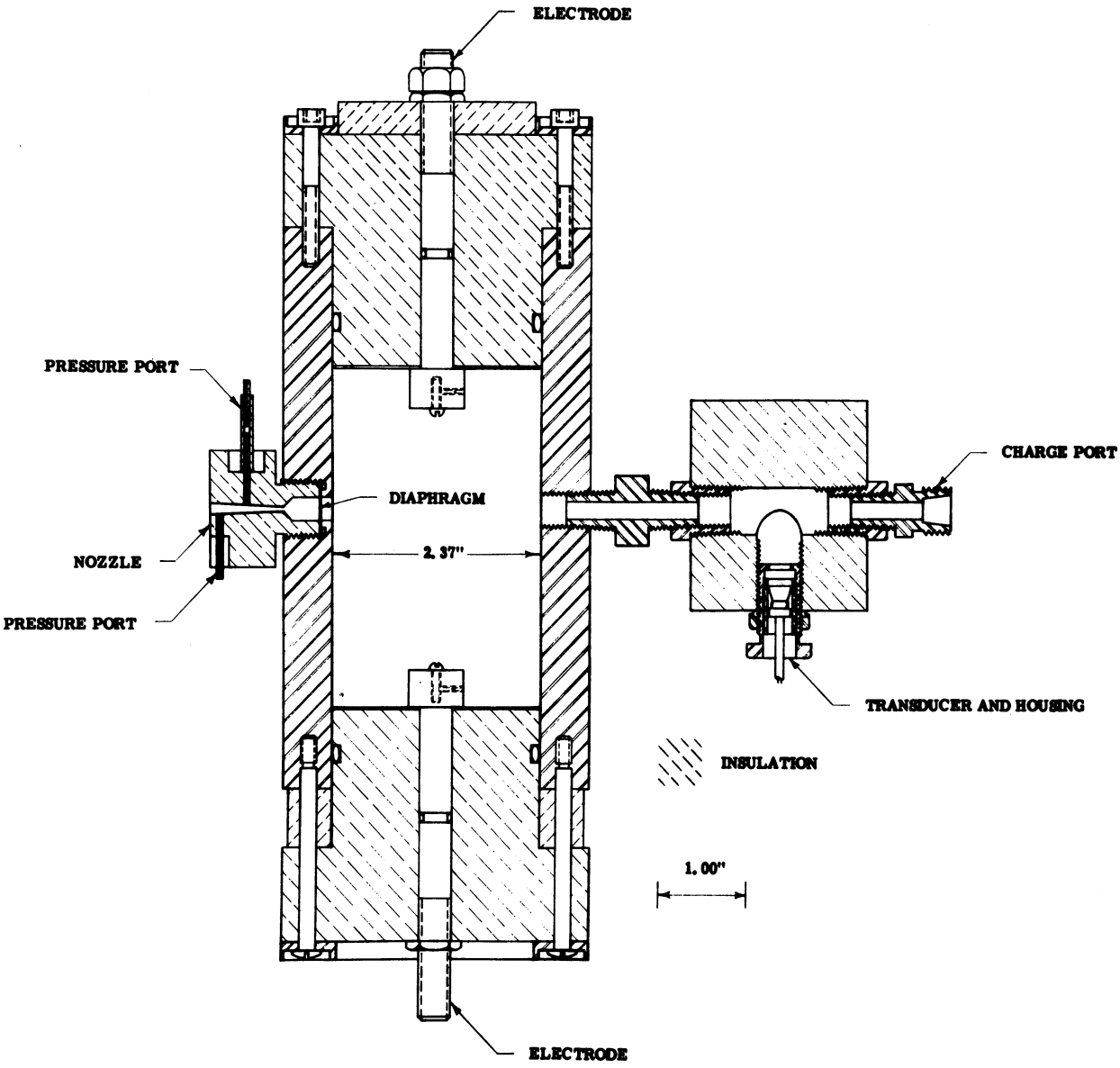

Figure 2. Schematic of Exploding Wire Chamber and Nozzle Arrangement.

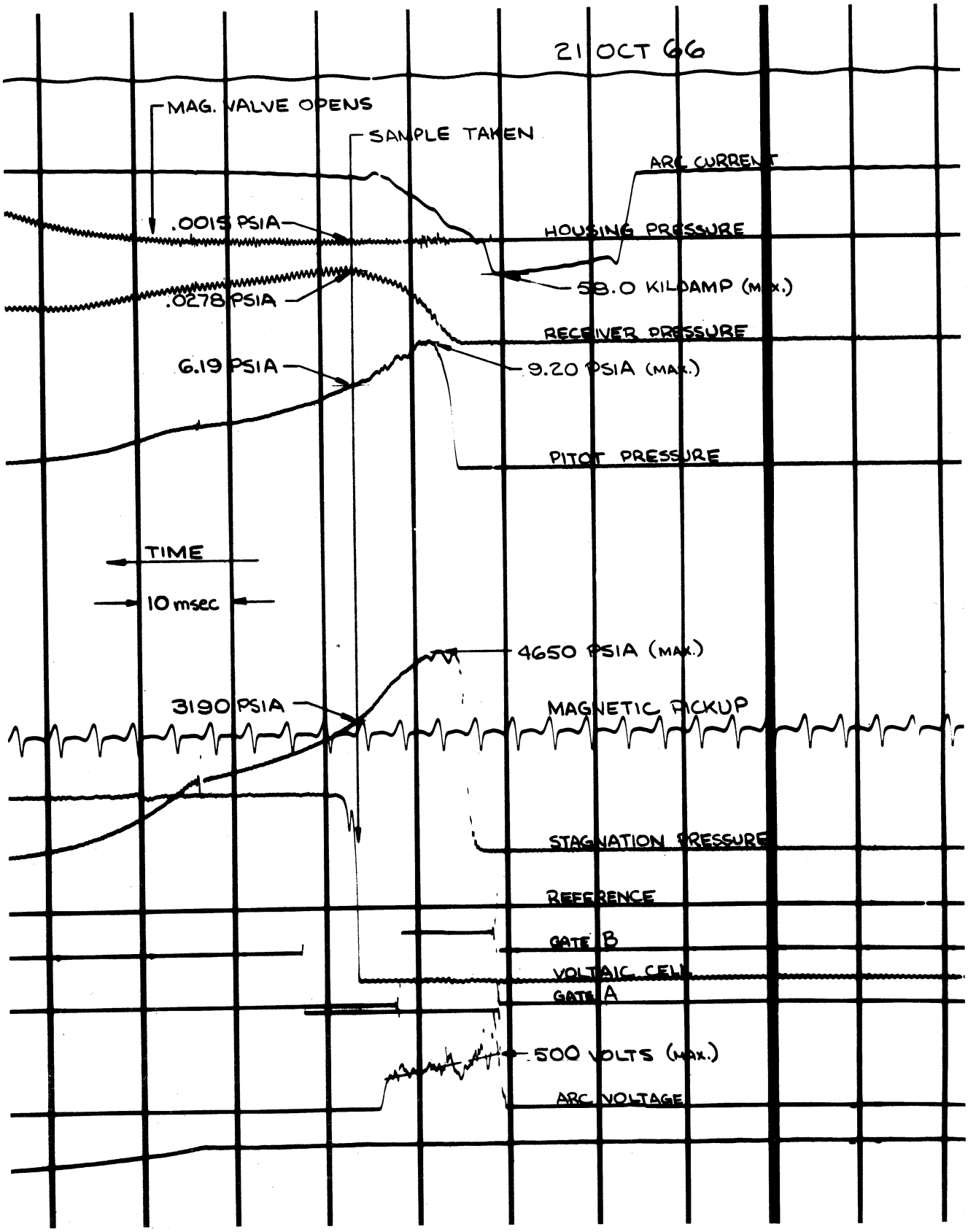

Figure 3. Oscillograph Trace of Typical Hot-shot.

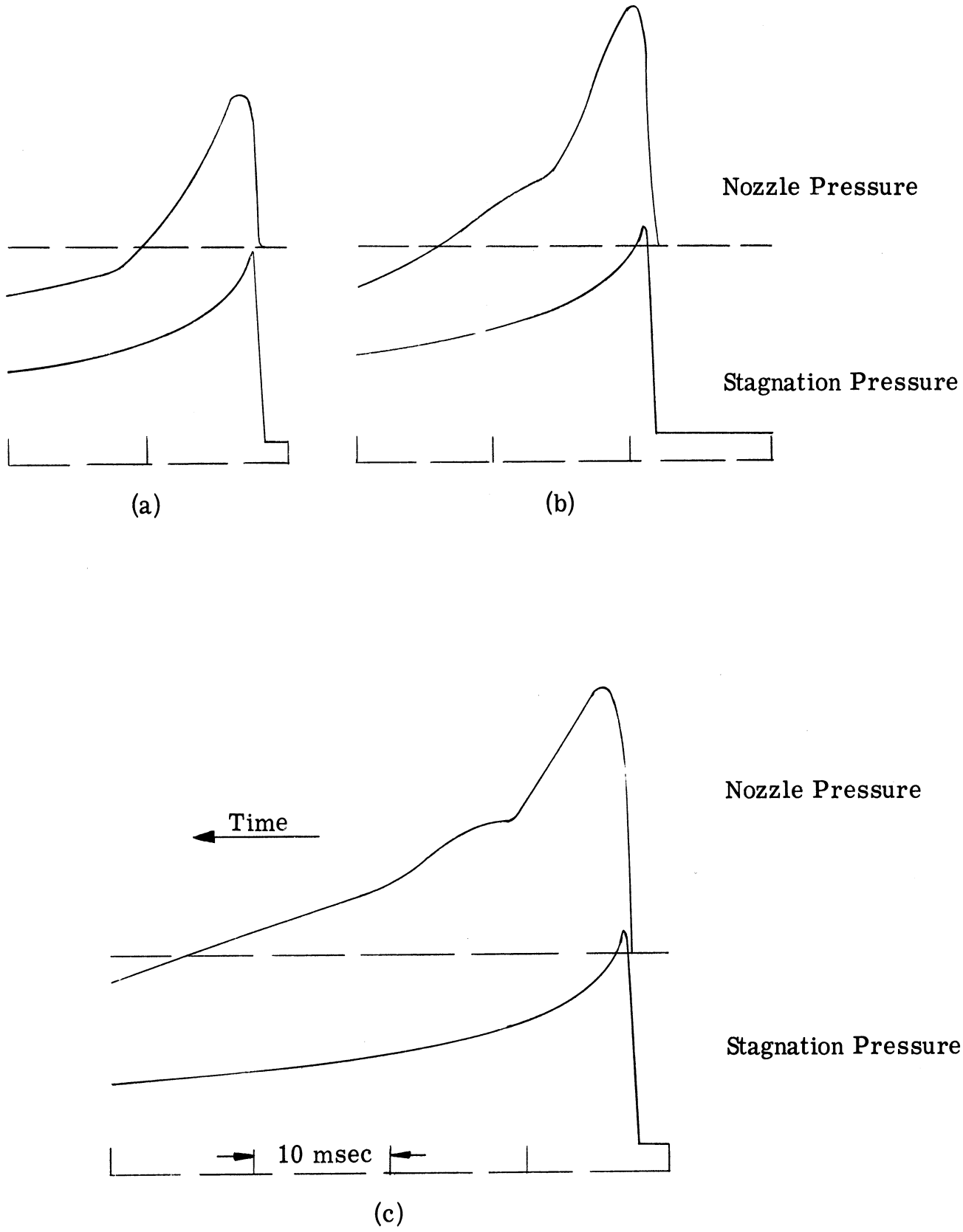

Figure 4. Oscillograph Traces of Three Exploding Wire Runs.

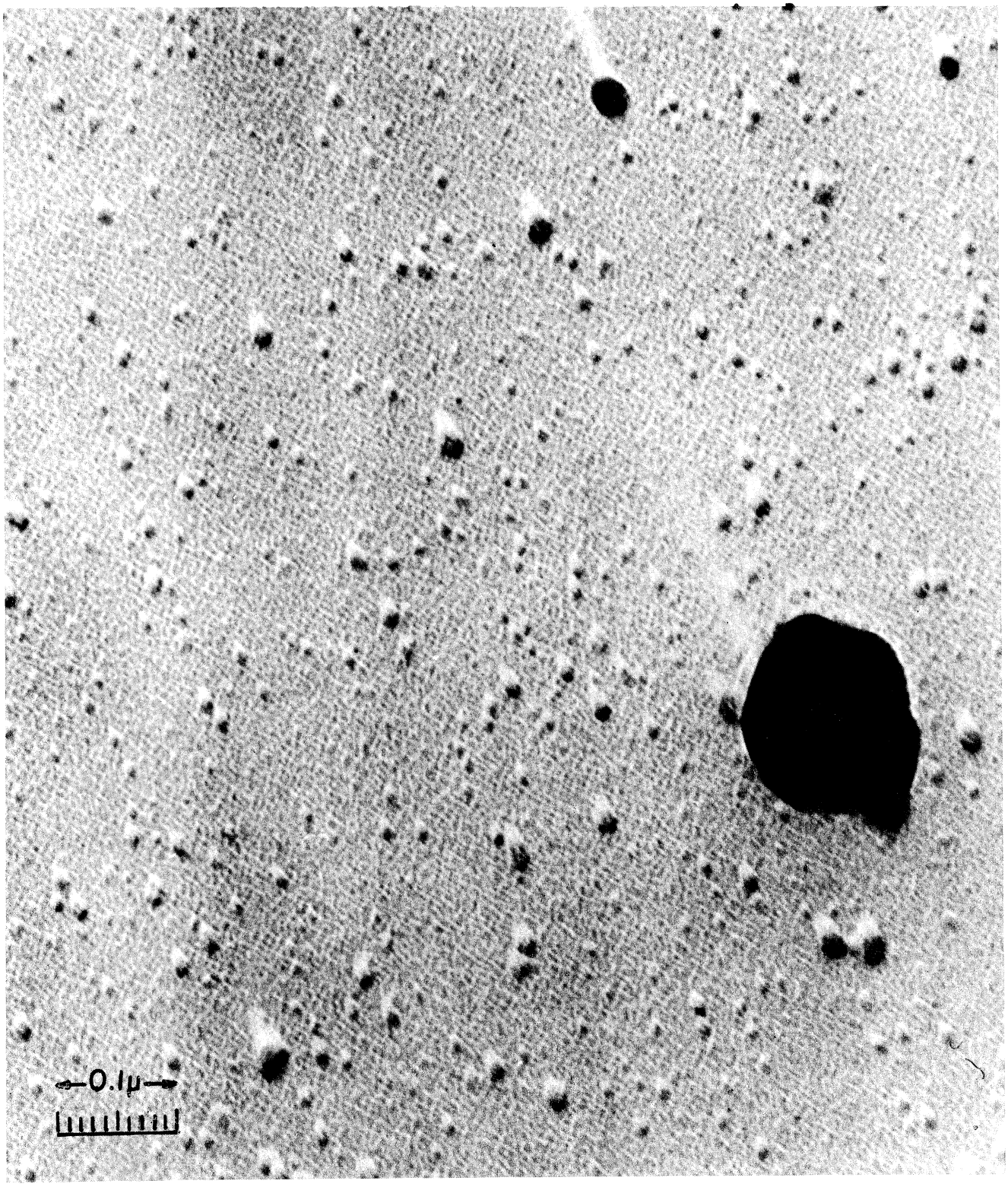

Figure 5. Photomicrograph of Particles Collected in Hot Shot. 216,000 X.

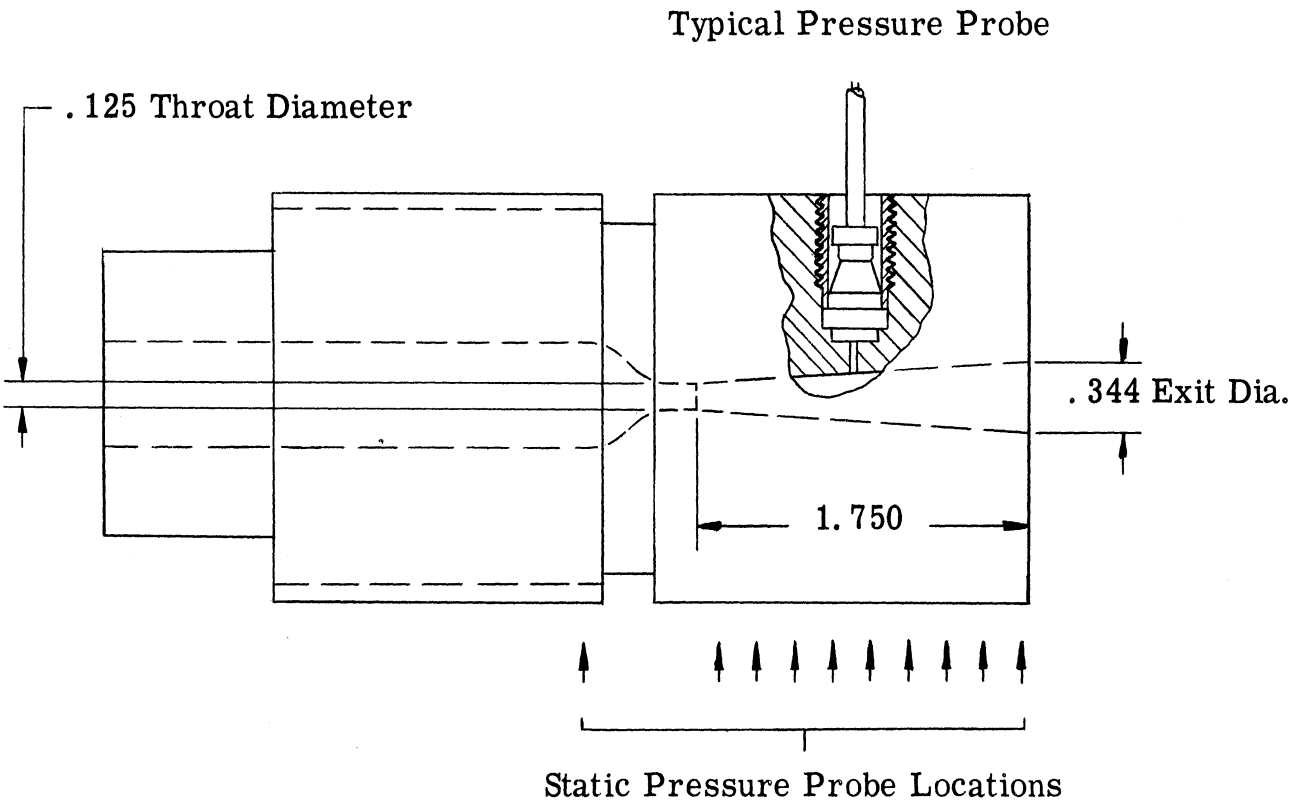

Figure 6. Mach 5 Nozzle

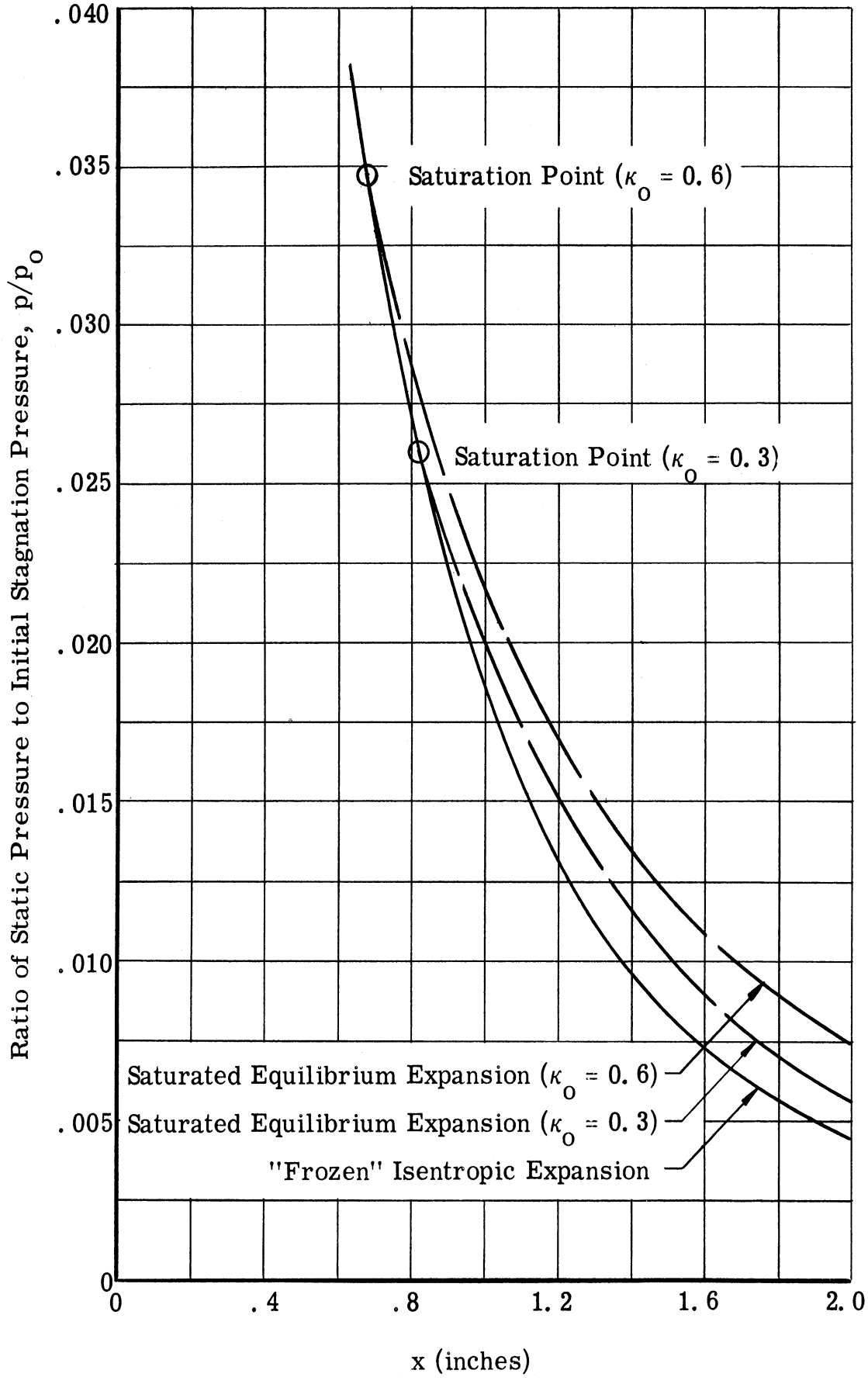

Figure 7. Mach 5 Nozzle Saturated Equilibrium Expansion (p_o = 4500 psia, T_o = 4500°K) (κ_o ≡ mass fraction of zinc)

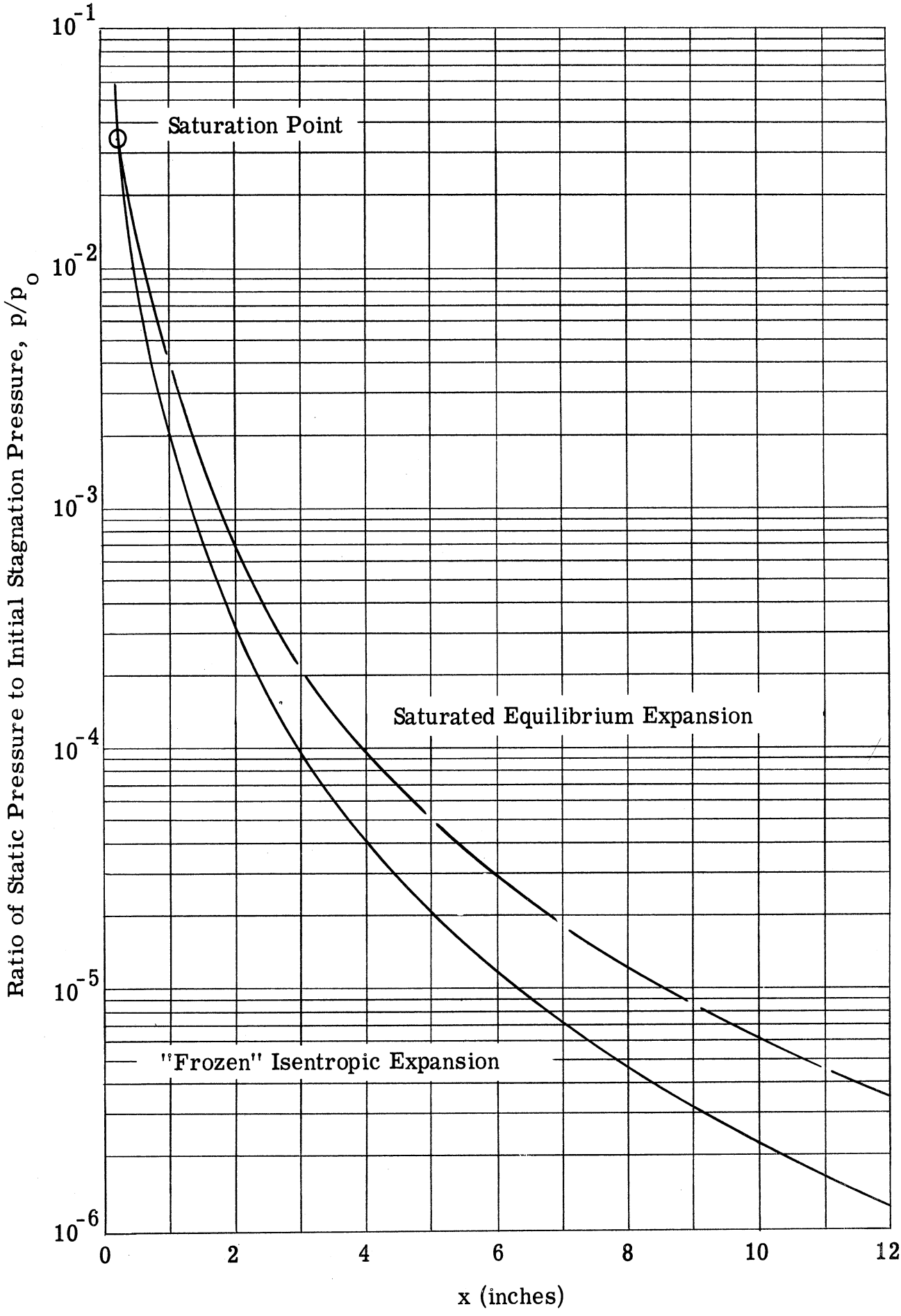

Figure 8. Mach 25 Nozzle Saturated Equilibrium Expansion (p_o = 4500 psia, T_o = 4500°K, mass fraction of zinc = 0.6)

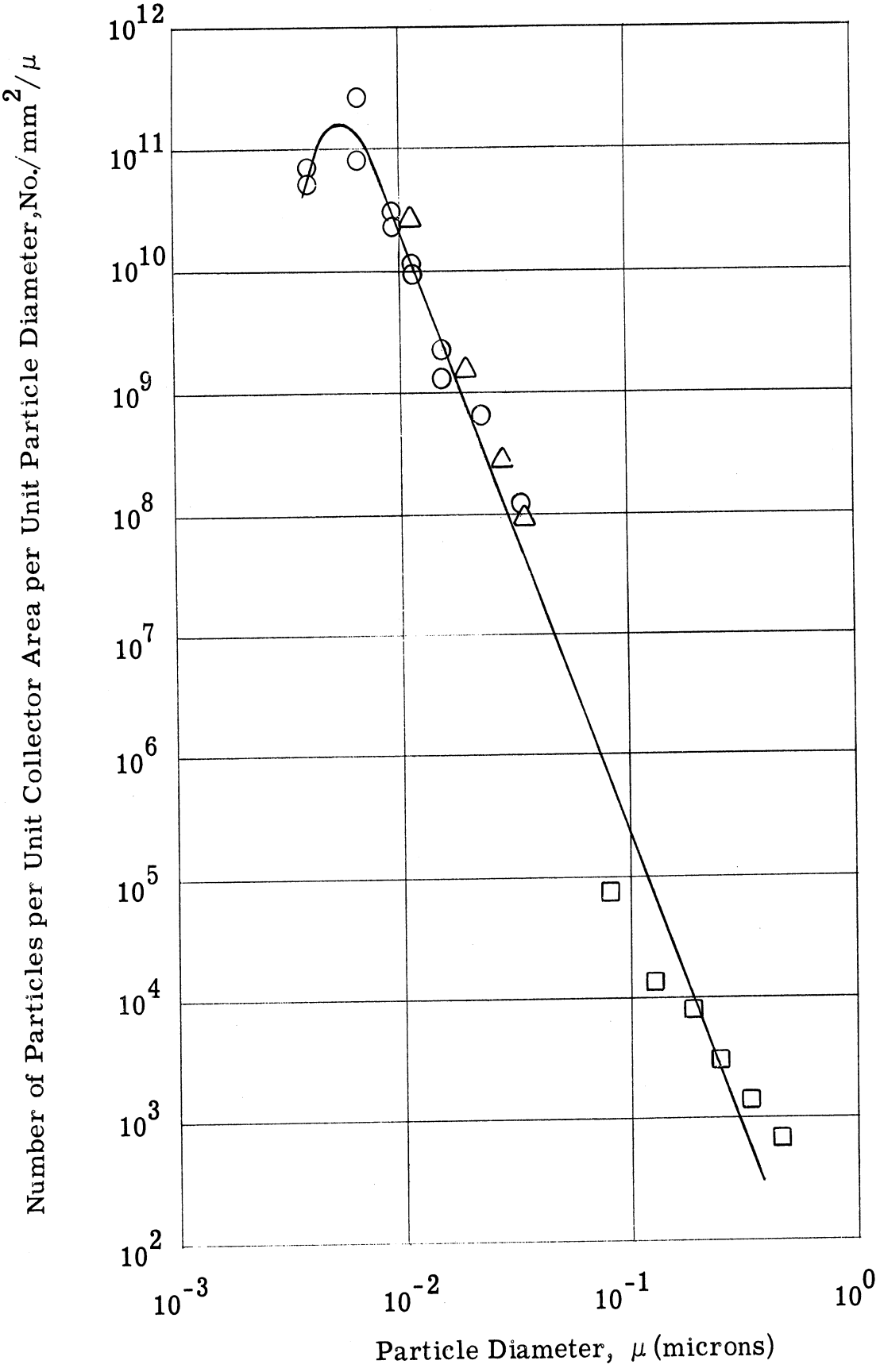

Figure 9. Particle Size Distribution Curve.

APPENDIX A. EXPLODING WIRE STUDY

An exploding wire was used as the metal vapor source in the study of condensation of metals. A metallic wire is vaporized by dissipating large amounts of stored energy of a capacitor in the wire and in the media in which the wire is exploded. This is accomplished by using the wire as the load of a low inductance L-R-C circuit. The vapor thus produced, then presents a good source of metal vapor for the study of condensation.

The wire was vaporized by dissipating the stored energy of the capacitor in an "optimum discharge." In this type of discharge, the wire vaporizes in the shortest time possible for a given circuit. It seems reasonable that the shorter the period of time, the more efficient would be the energy transfer to the wire. A short period also permits the approach to equilibrium with surrounding gas to occur with minimum delay.

"Optimum discharge" was the outcome of exploratory work on exploding wires which was undertaken to study the condensation of metal vapors. This work was done in two phases. During the first phase, wire "explosions" passed through the three regions of the exploding wire phenomenon which are known as the first pulse, dwell, and re-strike regions. The object of the initial series of experiments was to measure the energy deposited in the wire and in the medium in which the wire was exploded. This measurement yielded some qualitative information on the extent of vaporization of the wire. During the second phase of the work on the exploding wires, "optimum discharge" was obtained, and a limited amount of data was taken on it.

Since all of this work was of exploratory nature, the experiments were conducted in air at atmospheric pressure. A picture of the system is shown in Fig. A-1, and a schematic of the circuitry is shown in Fig. A-2. A 14.7 μfd/20KV Sangamo capacitor was used as the energy storage capacitor, and it was charged with a 0-30KV/10ma Sorenson Power Supply to a specified voltage V_0. The circuit inductance and resistance, exclusive of the wire, were approximately 0.50 μhy and 10.76 milliohm respectively. Of this resistance, 2.43 milliohm was contributed by the T and M non-inductive current shunt which was used to measure the current in the circuit as a function of time. The voltage across the wire was measured as a function of time with a P-6015 Tektronix High Voltage Probe. Both the voltage and current traces were recorded on a Type 551 Dual Beam Oscilloscope. The oscilloscope was triggered externally with the voltage signal induced on a pick-up coil which was located in the vicinity of the circuit.

A mechanical "drop-switch" was used to close the circuit. One contact of the switch, which was tied to a string, was dropped manually onto the positive terminal of the capacitor. This type of switch was chosen for the sake of its simplicity. Factors such as the inductance of the switch, and the energy loss in the switch were considered negligible.

The First Phase of Exploding Wire Study

The characteristic voltage and current traces for the wire "explosions" are shown in Fig. A-3. The periods, I, II, and III, are known as the first

pulse, dwell, and re-strike periods. The phenomena that take place during these periods have been discussed extensively by many authors, see Ref. A-1. When the switch is closed, the wire is rapidly heated as the current increases. It melts and vaporizes. The conductivity of the wire decreases rapidly as it goes into the vapor phase and current decreases to an undetectable value. During this period, which is the "first pulse," only a fraction of the capacitor energy is dissipated. The voltage pertaining to the remainder of the stored energy appears as a constant during passage through the second region which is designated as the "dwell" region. The magnitude of current in the circuit during this period is negligible. The vapor column constitutes a dense media. The voltage across the gap is not high enough to strike an arc in it. As the metal vapor column expands during the dwell region, the density decreases. By the end of the dwell period, the condition in the gap is such that the voltage across the gap strikes an arc in the expanding column. The remainder of the stored energy then discharges through the medium in an underdamped oscillatory manner. This period is referred to as the "re-strike" region.

The energy in the first pulse was calculated by integrating the v(t) x i(t) over time. In Fig. A-4, energy in the first pulse versus wire cross-section area is plotted for different wire lengths and for different initial stored energy of the capacitor. First pulse duration and dwell time versus cross-section area for the same variables are plotted in Figs. A-5 and A-6. Finally, first pulse energy and first pulse duration versus capacitor charging voltage for a constant wire diameter and length are plotted in Figs. A-7 and A-8.

The following observations were made from these experiments: (1) under certain conditions, energy in the first pulse approached to the initial stored energy of the capacitor, and re-strike never took place; (2) first pulse duration was shorter for wires which had shorter length, smaller cross-sectional area; and, for higher charging voltages, and (3) dwell time varied from 0 to a few hundred microseconds with variation of any one of the parameters (length, diameter, capacitor charging voltage) mentioned.

The energy transferred to the system during the first pulse causes the wire to vaporize, while the energy transferred during the re-strike ionizes the medium, and may heat the vapor-gas mixture to higher temperatures. However, since the re-strike takes place a long time after the first pulse in many cases, the vapor-gas mixture temperature decreases during the dwell and it is not determined how effective this secondary energy addition to the system is during the re-strike region in raising the temperature of the mixture above those attained in the first pulse. Therefore, work on exploding wires was carried on further to determine the conditions under which all of the stored energy of the capacitor can be dissipated during the first pulse whereby dwell and re-strike regions are eliminated. This type of discharge is herein called an "optimum discharge."

Second Phase of Exploding Wire Study (Optimum Discharge)

"Optimum discharge" characteristics were reported in Ref. A-2. In this type of discharge all of the stored energy of the capacitor is dissipated

during the first pulse. Both the voltage and current traces diminish to zero steadily by the end of the pulse which indicates that there is no more energy left in the capacitor, see Fig. A-9.

In order to understand the conditions under which the "optimum discharge" takes place, consider the voltage and current traces shown in Figs. A-10a through A-10f. In these figures, voltage and current traces are shown for 2.5 in. long, .010 in. dia Cu wire for different capacitor charging voltage V_o. At V_o = 0.300 KV, the discharge is an underdamped oscillatory discharge in which the wire does not break. At V_o = 1.5 KV the wire breaks and the discharge lasts for a shorter period. At V_o = 2.7 KV, the discharge is an "optimum discharge" in which both the voltage and the current values reach zero at the end of the first pulse. At V_o = 3.5 KV, there are the "first pulse" and the "dwell" periods, but re-strike does not take place. There is some energy left in the capacitor at the end of the discharge. At V_o = 5.0 KV, a classical wire explosion takes place with first pulse, dwell and re-strike periods. As the capacitor voltage is raised further, the dwell period becomes shorter, and at V_o = 10 KV, re-strike takes place before the end of the first pulse, in which the dwell period does not exist. At this voltage level for this case, the voltage gradient which is developed across the wire is high. The gas surrounding the wire cannot hold such high voltage; therefore, an arc strikes on the periphery of the wire which results in this early re-strike.

When this series of experiments is conducted on any other wire with a given diameter and length, similar voltage and current traces are obtained as a function of capacitor charging voltage. The results of the experiments indicated that the voltage at which the "optimum discharge" takes place is directly proportional to the wire cross-section area, and it is independent of the wire length. The wire diameter was varied from 7.5×10^{-6} to 5×10^{-4} $in.^2$ and wire length was varied from 1 to 7 in. Experiments were conducted using Pt, Cu, Ag and Zn wires. In Fig. A-11, capacitor charging voltage for optimum discharge, V_o, is plotted versus wire cross-section area for wires of these metals. The wire lengths for most of the datum points were varied from 1 to 7 in. while keeping the wire cross-section area constant. In Fig. A-12, optimum discharge voltage versus the wire cross-section area is plotted for copper wires which were exploded using one and two capacitors (capacitors in the latter case were connected in parallel).

While the capacitor charging voltage for "optimum discharge" in a given wire diameter remains constant for different wire lengths, the time dependent voltage and current traces vary with the wire length. In Figs. A-13a through A-13d voltage and current traces are shown for .016 in. dia Ag wire. The optimum discharge voltage for wire of this diameter was 5.7 KV and it was kept constant in these experiments, while the wire length was varied from 1 to 7 in. As the wire length is increased, the duration of the pulse increases from 4.8 to 8 μsec (half cycle of the characteristic oscillations in the

circuit was 8.5 μsec), the peak voltage across the wire decreases from 16 to 3.5 KV, and the current in the circuit decreases from 29.6 to 23.9 KA.

The peak voltage across the wire becomes very large as the wire is shortened, and this high voltage causes a peripheral arc in the gap (the length of the gap between the wire holders is the same as the wire length) if the conditions in the gap are such that high voltage cannot be sustained across it. Under these conditions, the dissipation of the energy of the capacitor is no longer completed in one pulse, and the discharge continues in an underdamped oscillatory manner. The voltage and current traces for such a discharge are shown in Fig. A-14. The wire was 1 in. long, No. 24 Cu, and the capacitor was charged to its "optimum discharge" voltage, 9.6 KV. Arcing occurred in the gap at 4.3 μsec. This arcing is inferred only from the voltage and current traces, and arcing has been observed in similar cases by streak photographs reported in Ref. A-3. In conclusion, peripheral arcing in the gap limits the "optimum discharge" to wires longer than a certain minimum length in which the arcing takes place. The "optimum discharge" in wires longer than 7 in. was not investigated.

REFERENCES

A-1 Chase, W. G. and Moore, H. K., ed., Exploding Wires, Vol. I, II, and III, Plenum Press, New York, 1959, 1962, 1964.

A-2 Oktay, Erol, "Effect of Wire Cross Section on the First Pulse of an Exploding Wire," The Review of Scientific Instruments, Vol. 36, No. 9, Sept. 1965.

A-3 Edelson, H. D. and Korneff, T., "Conducting Mechanism for Exploding Wires in a Vacuum," Exploding Wires, Vol. 3, 1962.

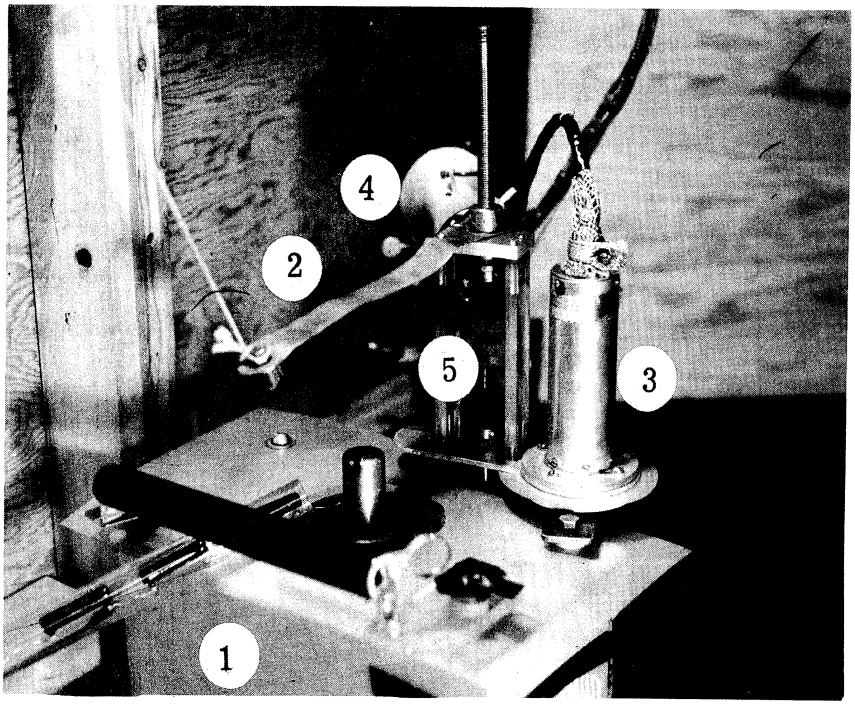

Figure A-1. Exploding Wire System

1. Capacitor
2. "Drop" Switch
3. Current Shunt
4. Voltage Probe
5. Exploding Wire

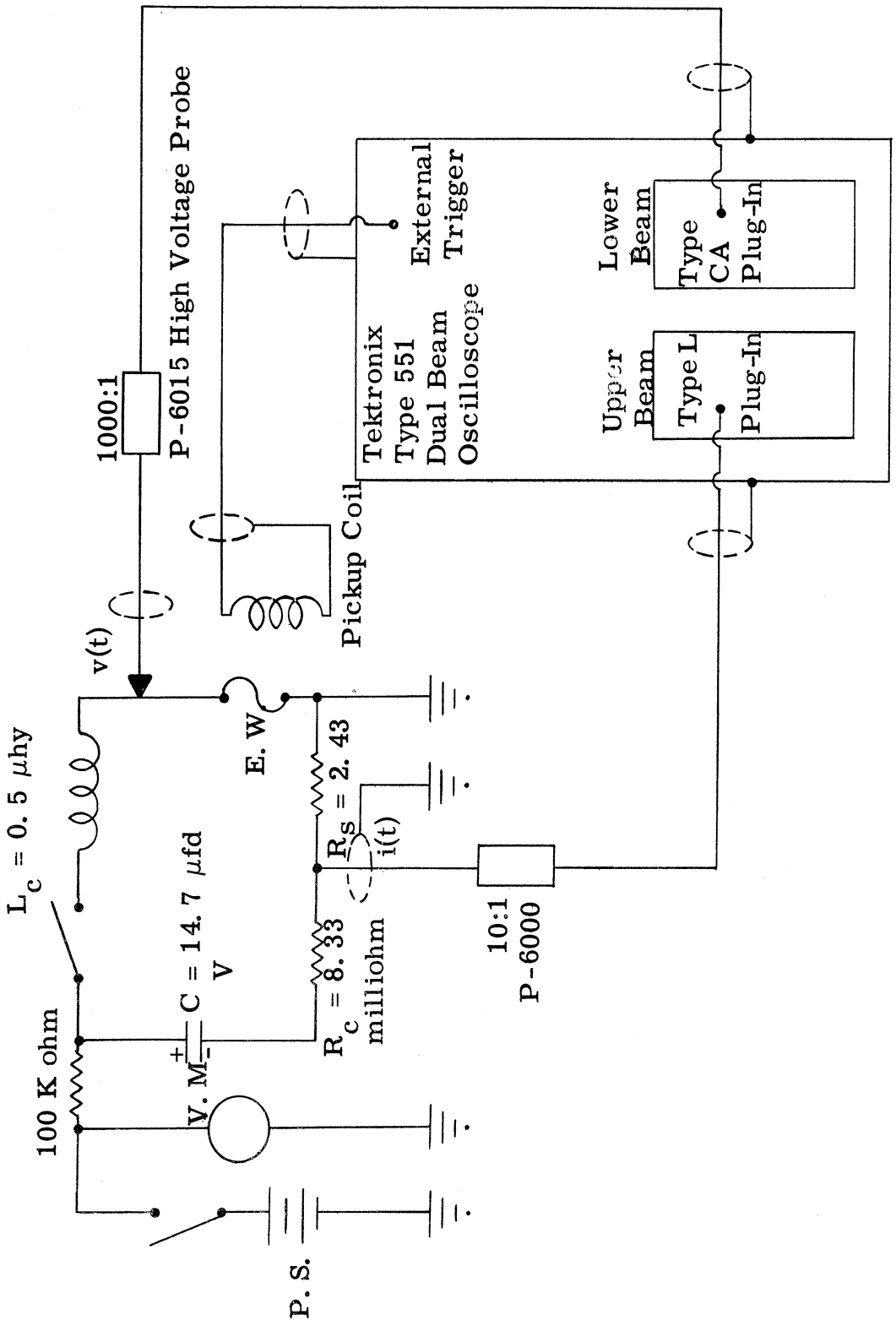

Figure A-2. Exploding Wire Circuitry

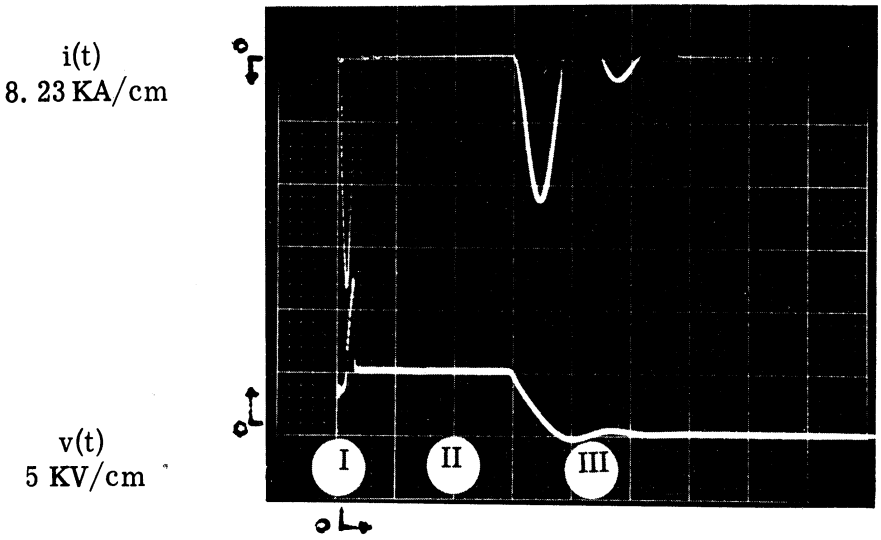

Figure A-3. Voltage and Current Traces for the Characteristic Wire Explosions with First Pulse, Dwell, and Re-Strike

(4 in. long, No. 28 Cu Wire, C = 14.7 μfd, V = 8 KV)

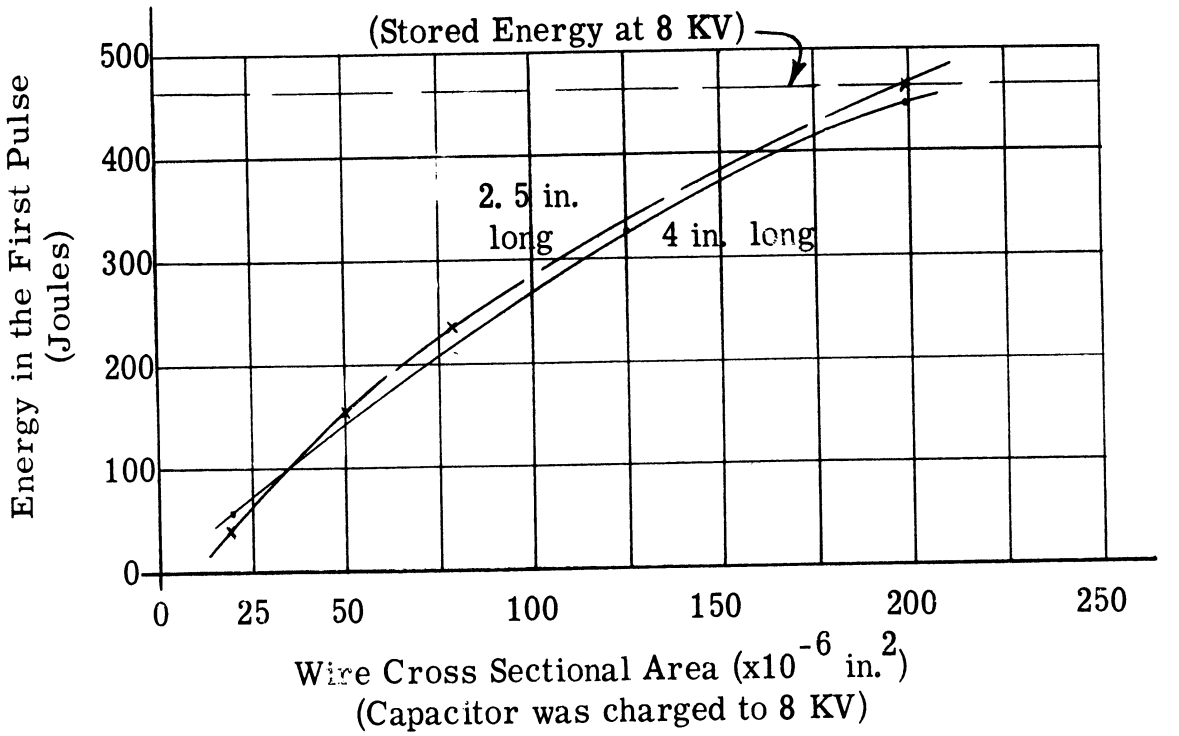

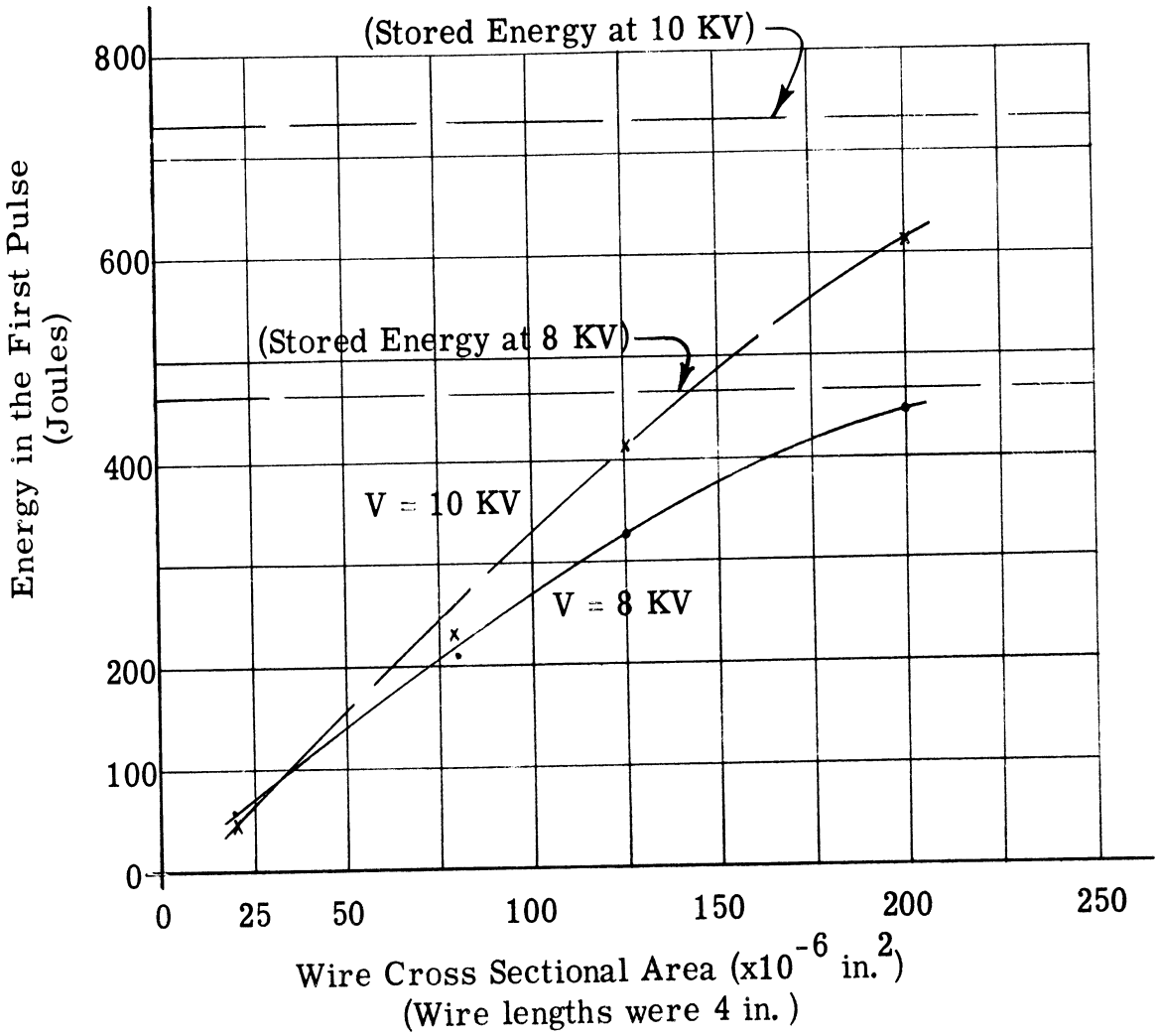

Figure A-4. First Pulse Energy Versus Wire Cross Sectional Area for Different Wire Lengths and Capacitor Charging Voltages (Cu Wire, C = 14.7 μfd)

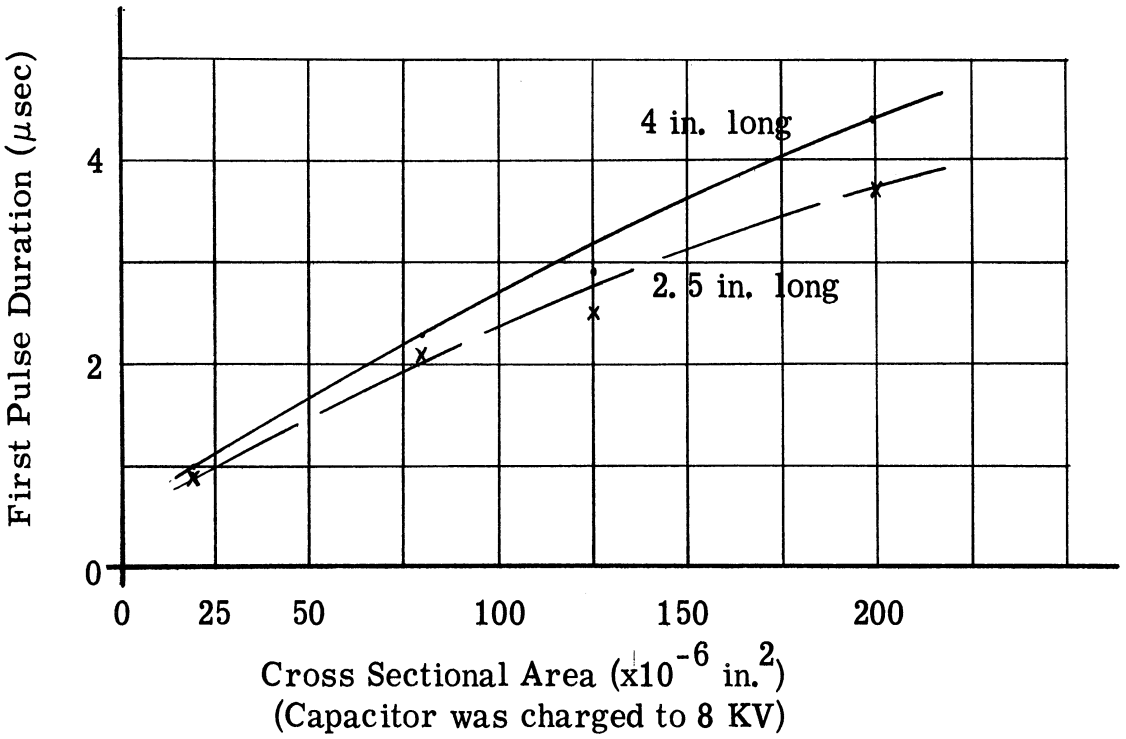

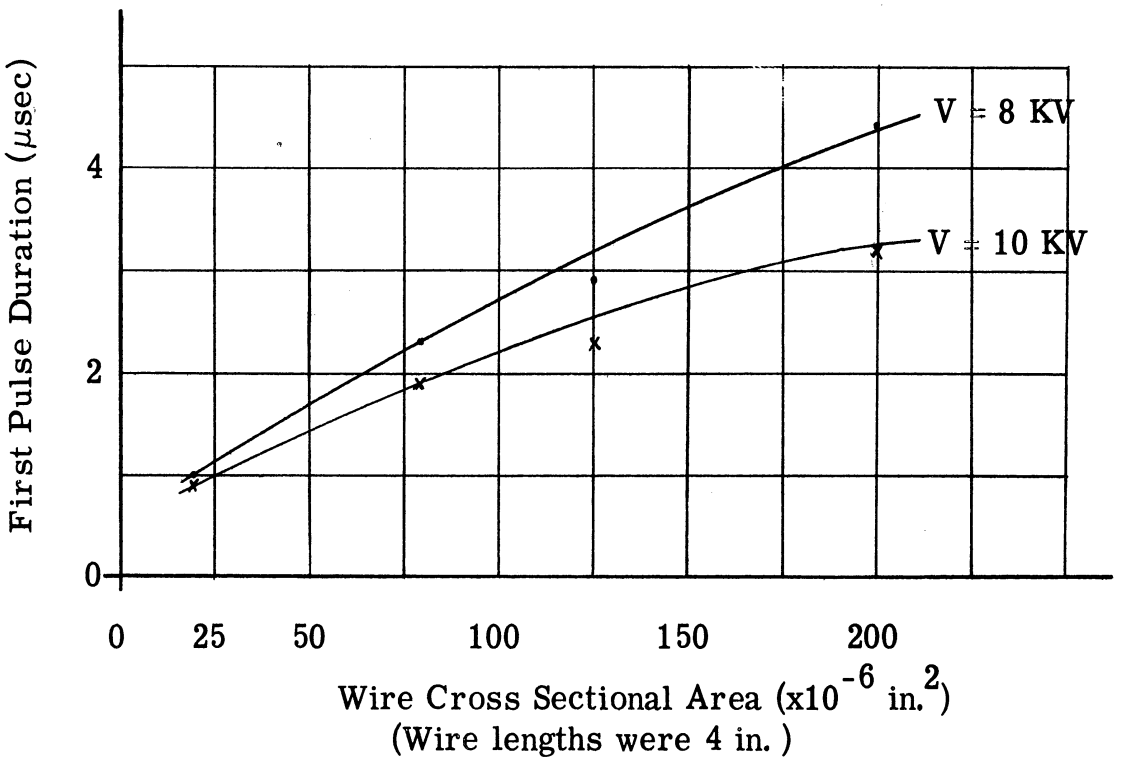

Figure A-5. First Pulse Duration Versus Wire Cross Sectional Area for Different Wire Lengths and Capacitors Charging Voltage (Cu Wire, C = 14.7 μfd)

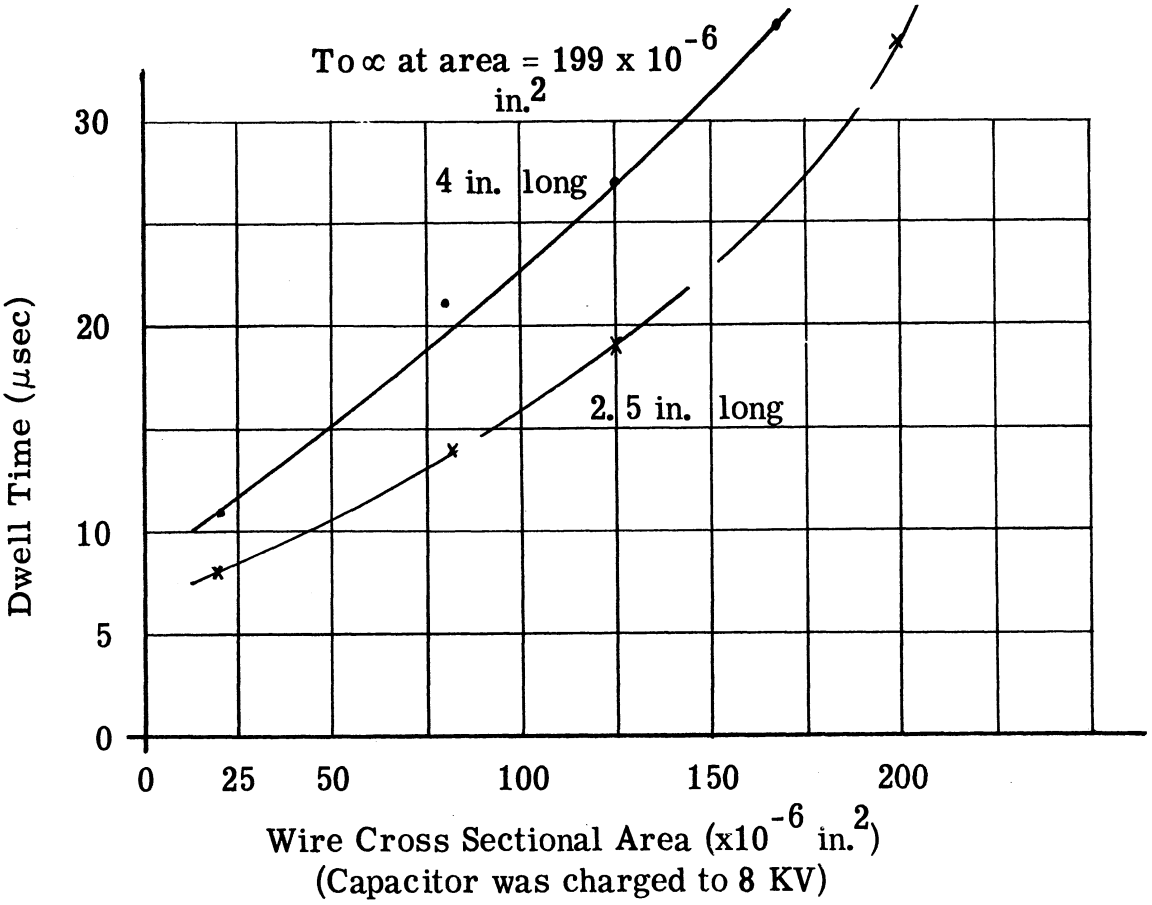

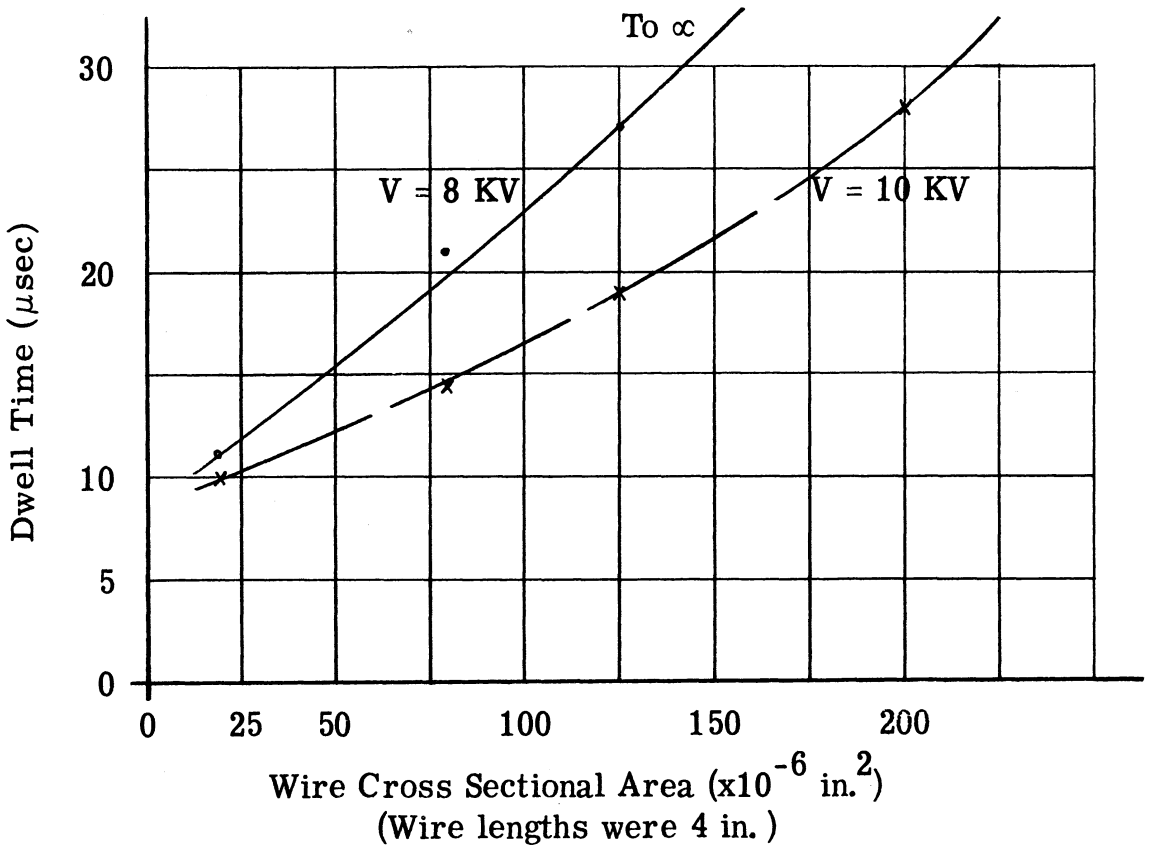

Figure A-6. Dwell Time Versus Wire Cross Sectional Area for Different Wire Lengths and Capacitor Charging Voltage (Cu Wire, C = 14.7 μfd)

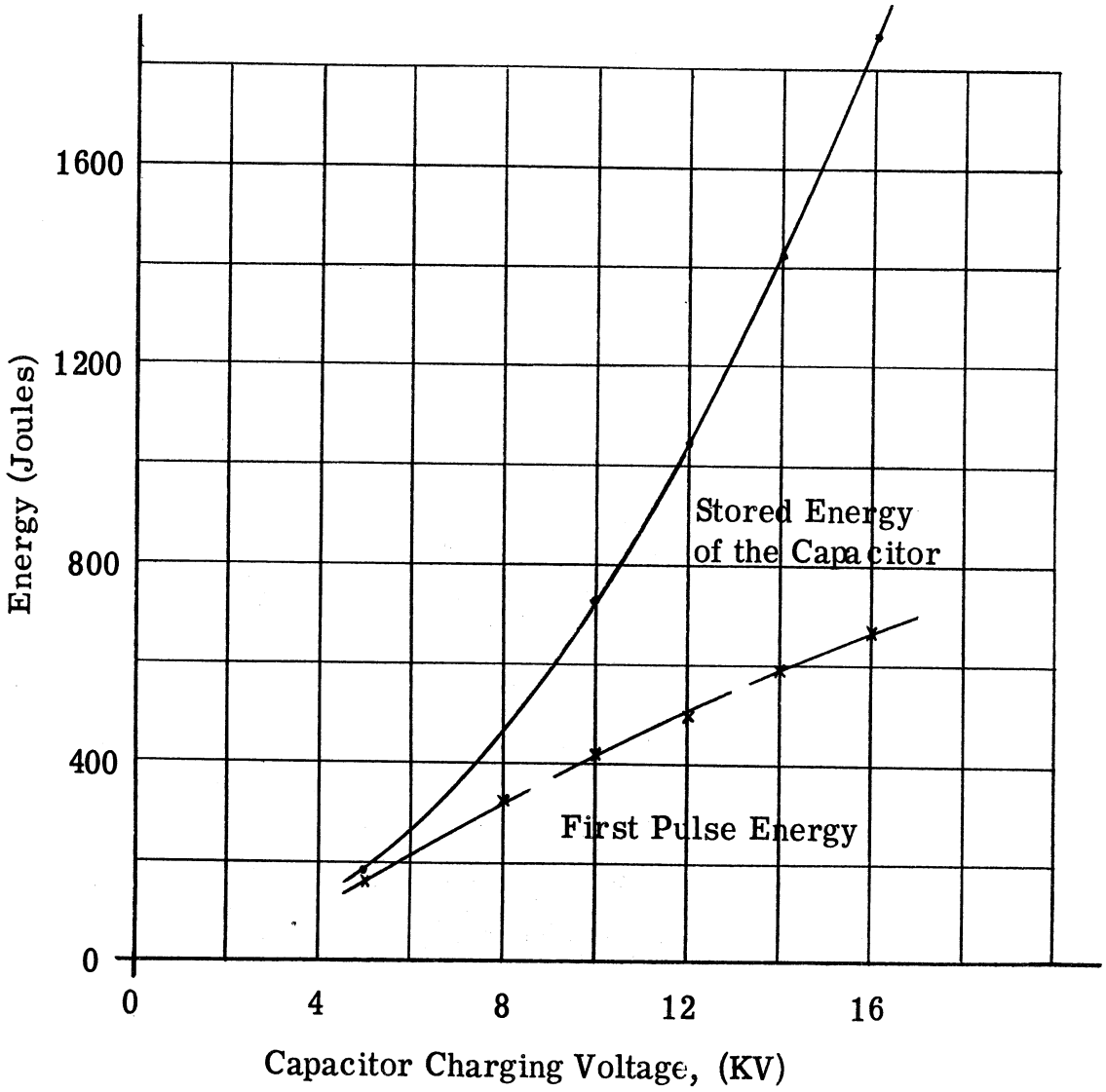

Figure A-7. First Pulse Energy Versus Capacitor Charging Voltage (4 in. long, No. 28 Cu Wire, C = 14.7 μfd)

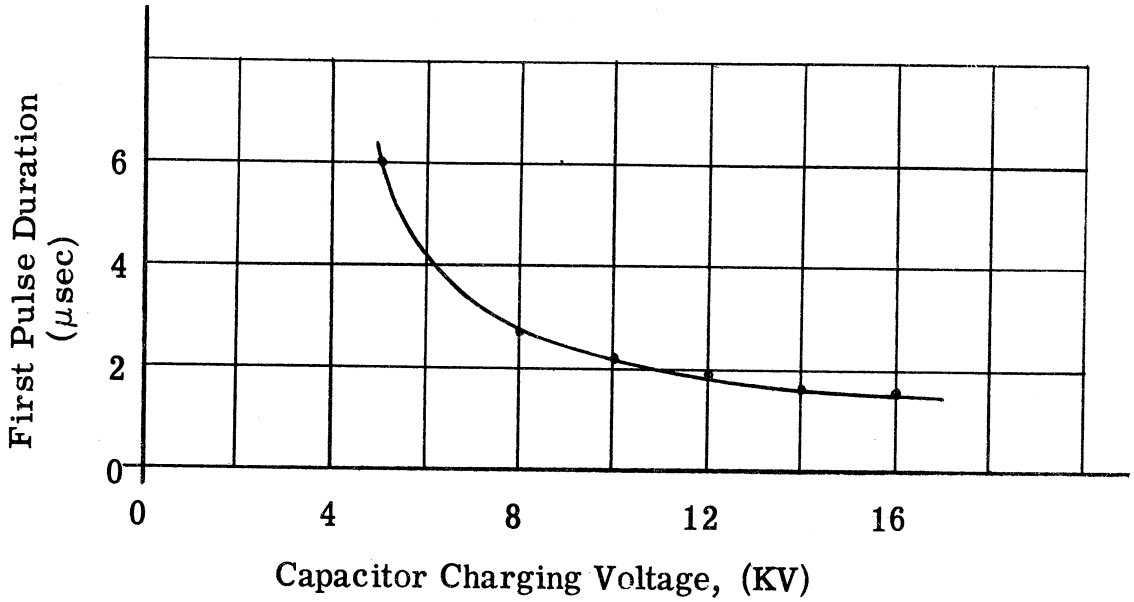

Figure A-8. First Pulse Duration Versus Capacitor Charging Voltage (4 in. long, No. 28 Cu Wire, C = 14.7 μfd)

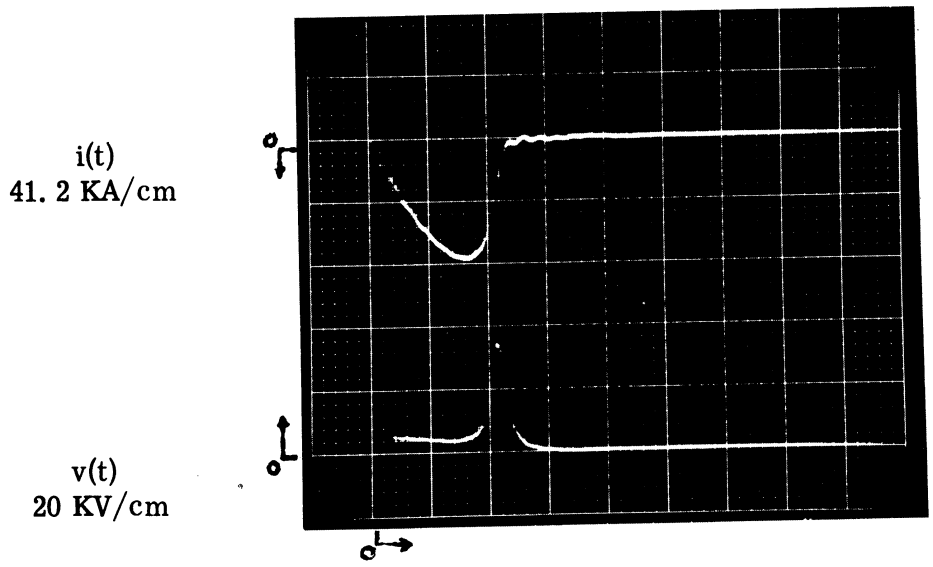

Figure A-9. Voltage and Current Traces for an Optimum Discharge (3 in. long, No. 22 Ag Wire, C = 14. 7 μfd, V_o = 15 KV)

Figure A-10. Current and Voltage Wave Forms as a Function of the Capacitor Charging Voltage, V, for a 2 1/2 in. long No. 30 Cu Wire

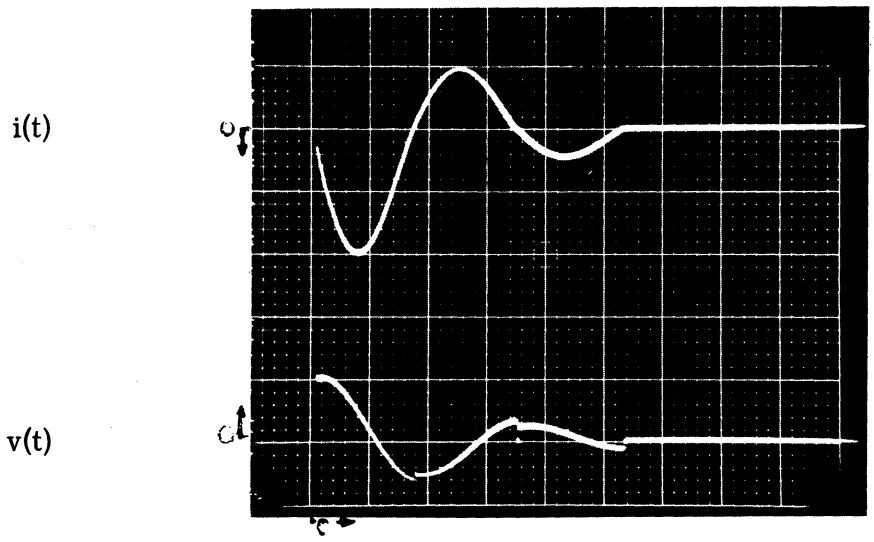

A-10a. 0.823 KA/cm, 0.100 KV/cm, 5 μsec/cm
V = 0.300 KV

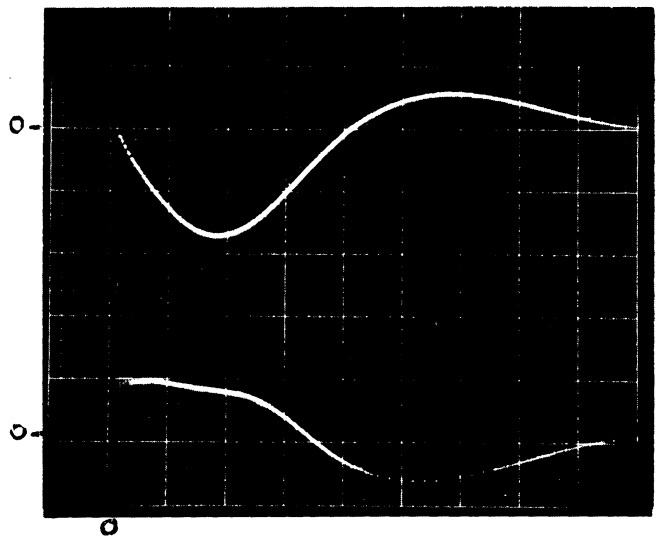

A-10b. 4.12 KA/cm, 0.500 KV/cm
2 μsec/cm, V = 1.5 KV
(wire broke off for the first time)

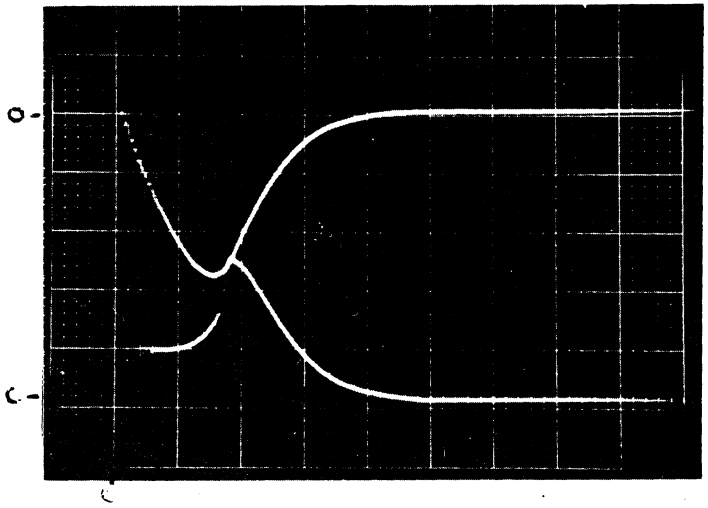

A-10c 4. 12 KA/CM, 1. 0 KV/CM, 2 μsec/CM
V_o = 2. 7 KV (Optimum discharge)

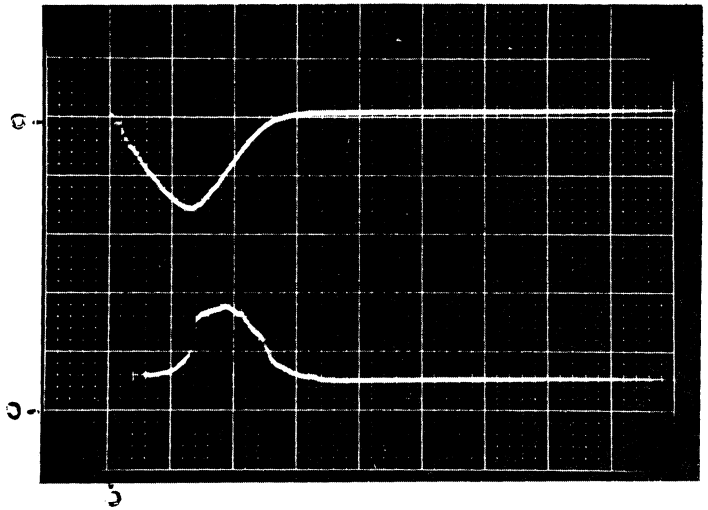

A-10d 8. 26 KA/CM, 2. 0 KV/CM, 2 μsec/CM
V_o = 3. 5 KV (No re-strike)

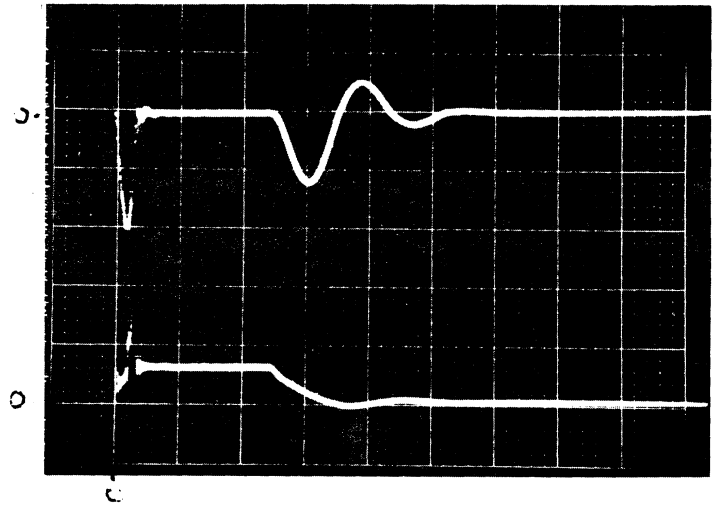

A-10e 8. 24 KA/CM, 5. 0 KV/CM, 10 μsec/CM
V_o = 5. 0 KV (Classical wave form)

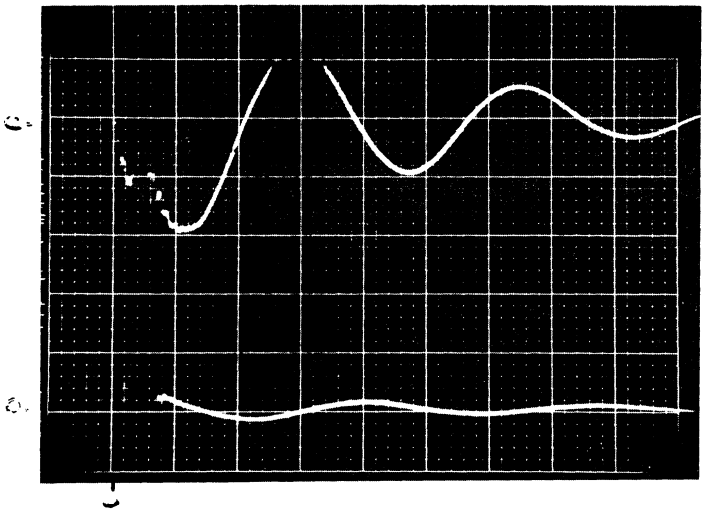

A-10f 20. 6 KA/CM, 10 KV/CM, 5 μsec/CM
V_o = 10 KV (No dwell)

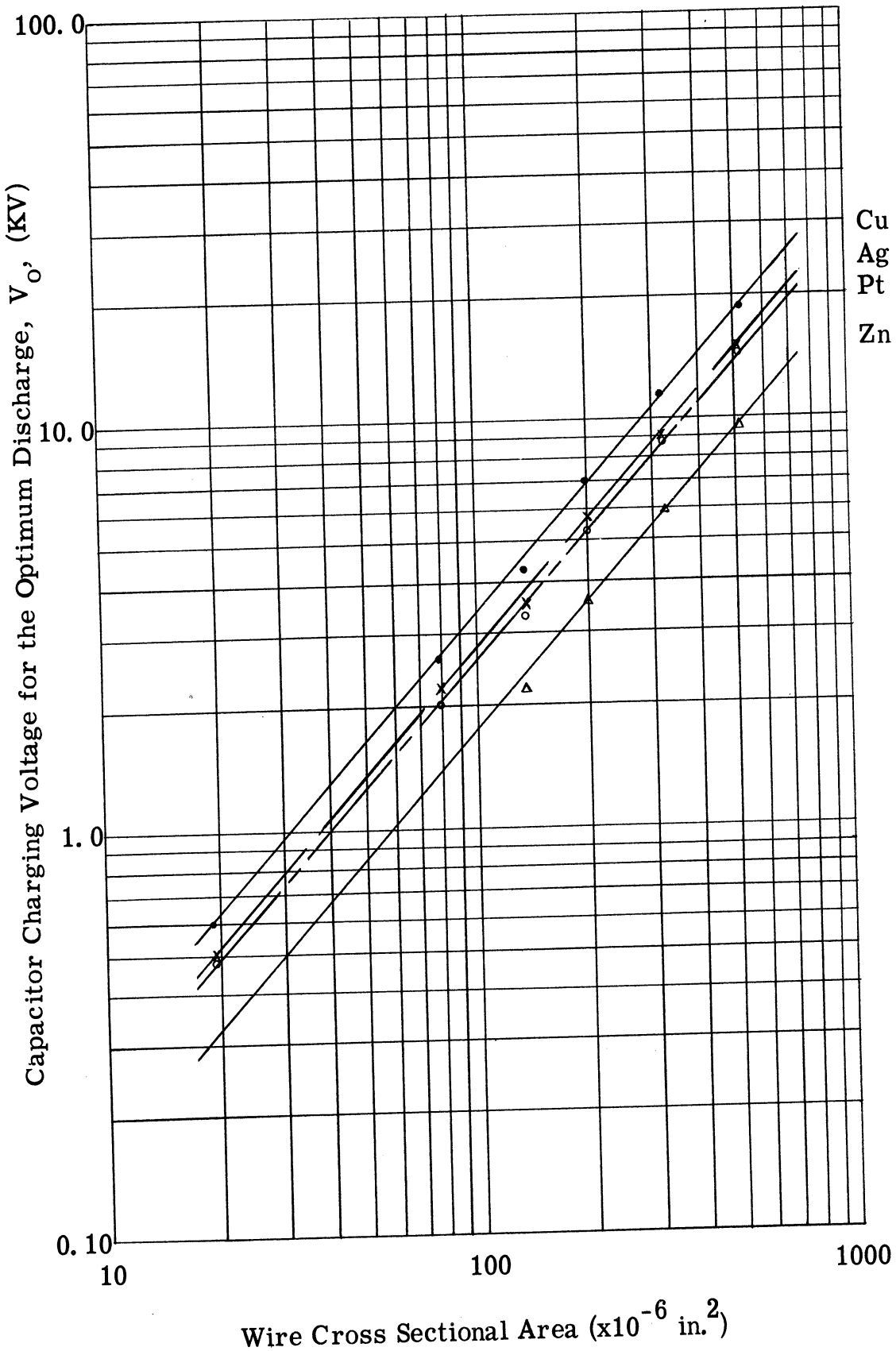

Figure A-11. Optimum Discharge Voltage Versus Wire Cross Sectional Area for Cu, Ag, Zn and Pt. (C = 14.7 μfd)

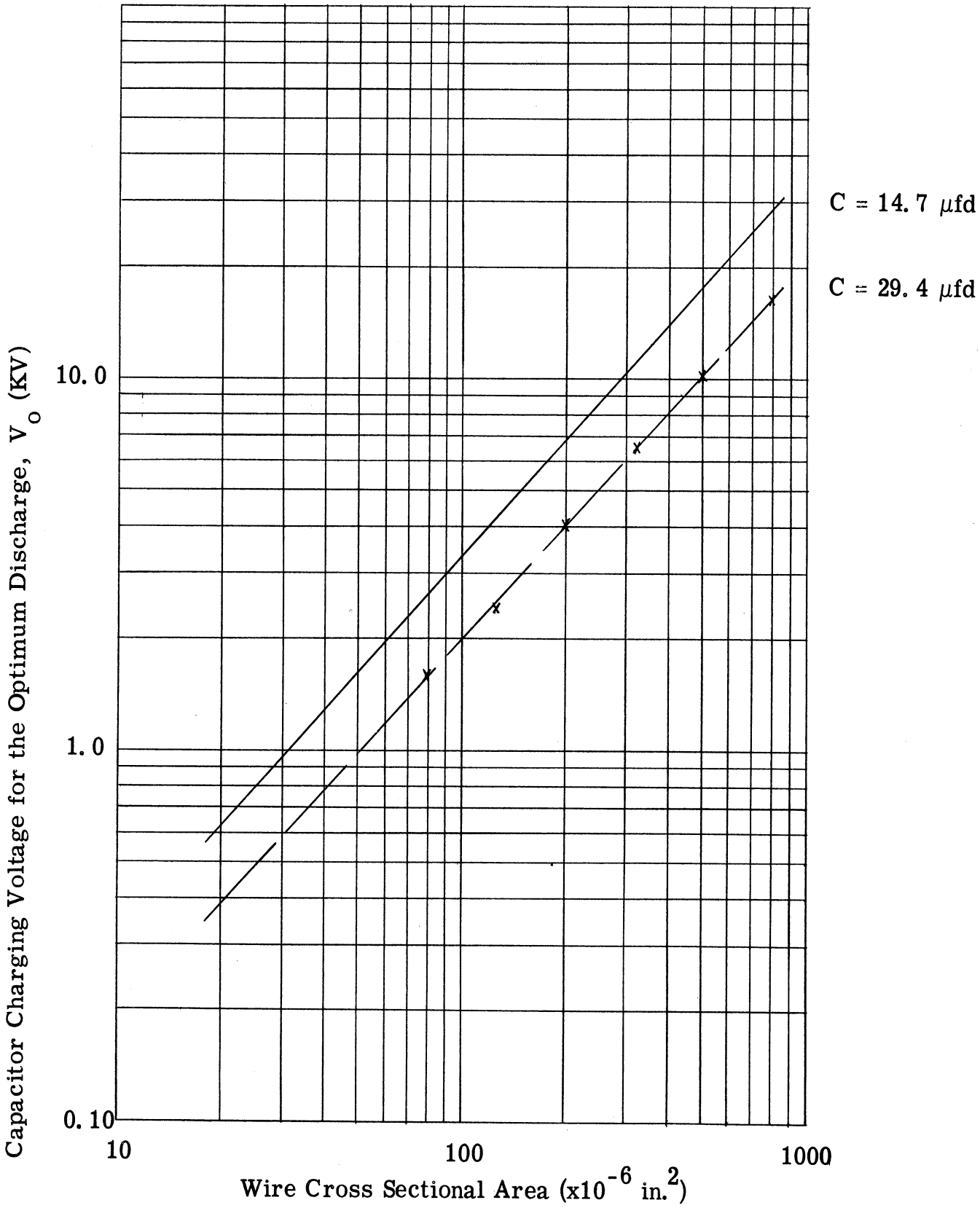

Figure A-12. Optimum Discharge Voltage Versus Wire Cross Sectional Area for Cu Wire for Different Energy Storage Capacitance

i(t)

v(t)

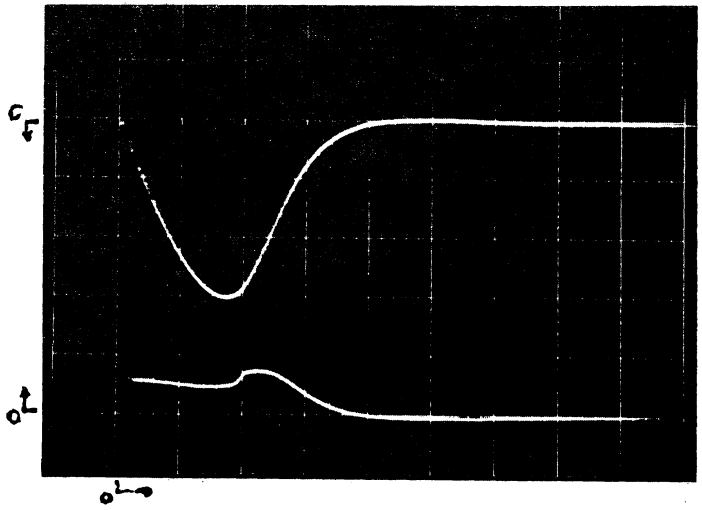

A-13a. (8. 23 KA/cm, 5 KV/cm) 7 inches long

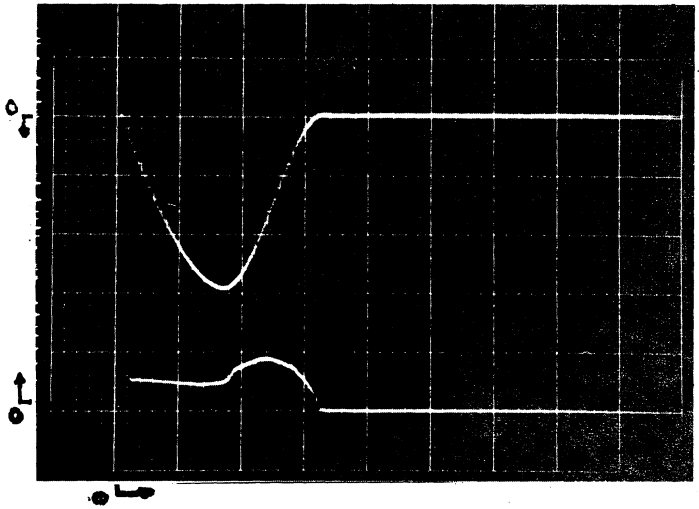

A-13b. (8. 23 KA/cm, 5 KV/cm) 5 inches long

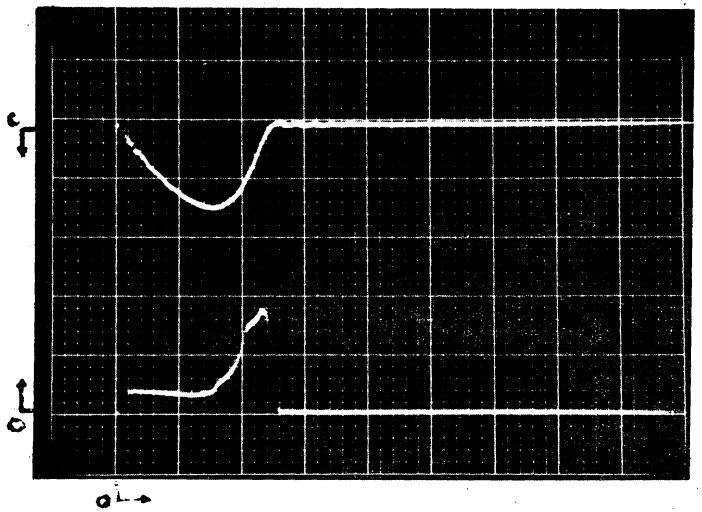

A-13c. (20. 5 KA/cm, 5 KV/cm) 3 inches long

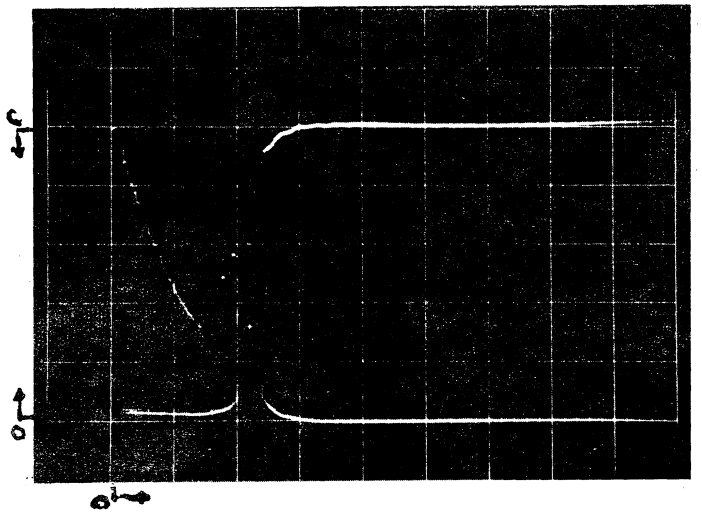

A-13d. (8. 23 KA/cm, 10 KV/cm) 1 inch long

Figure A-13. Voltage and Current Traces for Optimum Discharge for No. 26 Ag Wire, for Different Wire Length (C = 14. 7 μfd, V_o = 5. 7 KV, Sweep Time - 2 μsec/cm)

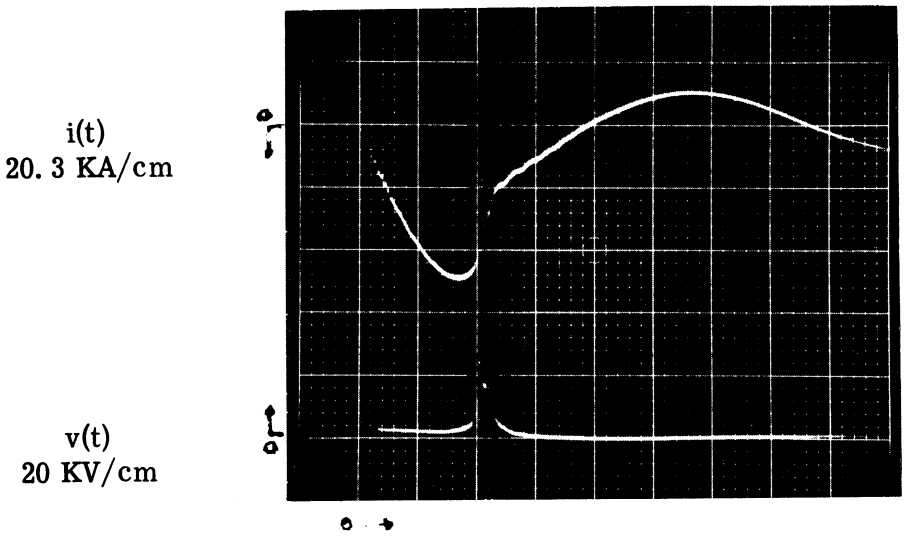

Figure A-14. Voltage and Current Traces for a Discharge in which Peripheral Arcing Occurred

(1 in., No. 24 Cu Wire, C = 14.7 μfd, V_o = 9.6 KV)

APPENDIX B. DESCRIPTION OF THE EXPLODING WIRE SYSTEM FOR THE STUDY OF CONDENSATION

The exploding wire system for the study of condensation consists of three parts:

(1) the exploding wire circuitry,

(2) the pressure chamber and the nozzle,

and (3) instrumentation to obtain electrical and pressure data.

A picture of the complete system is shown in Fig. B-1.

The Exploding Wire Circuitry

The schematic of the exploding wire circuitry is similar to the one shown in Fig. A-2. Two 14.7 μfd/20 KV capacitors connected in parallel are used as the energy storage capacitor.

Pressure Chamber and the Nozzle Assembly

A sketch of the stagnation chamber is shown in Fig. 2. The main body of the chamber is made of 3 1/2 in. O. D. seamless stell tubing which has a .625 in. wall thickness. The end parts of the chamber are made of delrin and the wire holders are made of 0.375 in. copper rod. The volume of the chamber was variable from about 13.6 to 17.8 $in.^3$ It was varied by moving the end plugs axially.

The nozzle was a separate piece which was screwed into the chamber. The pressure port at .075 in. from the exit plane was used to measure the nozzle pressure. The size of this port was varied. The diaphragm between the nozzle and the chamber was made of .005 in. thickmylar or .0075 in. thick kodapak.

Instrumentation

Two sets of measurements are made in this system: (1) current through the wire as a function of time, i(t), and voltage across the wire as a function of time, v(t), and (2) stagnation chamber and nozzle pressures as a function of time. The v(t) and i(t) traces are recorded on a dual beam Tektronix type 551 oscilloscope, and the pressure measurements are recorded on a 14 channel CEC oscillograph.

A block diagram of the pressure measurement system is shown in Fig. B-2. This schematic applies to both the stagnation and nozzle pressure measurements. The stagnation pressure is measured with a Microsystem 0-1000 psi bonded semi-conductor strain gage type of pressure transducer, while the nozzle pressure is measured with a Hidyne 0-30 psi variable reluctance pressure transducer. The Microsystem pressure transducer has a full bridge network in the transducer while the Hidyne pressure transducer has a half bridge network in it.

Both transducers are excited with the 30 KV 5 V source of the Plug-In system, and their outputs are de-modulated and amplified with the Plug-In amplifier unit. The output of these amplifiers is fed to the CEC Type galvanometer through an impedance matching network shown in the figure. The CEC is started manually just before the "drop switch" is closed.

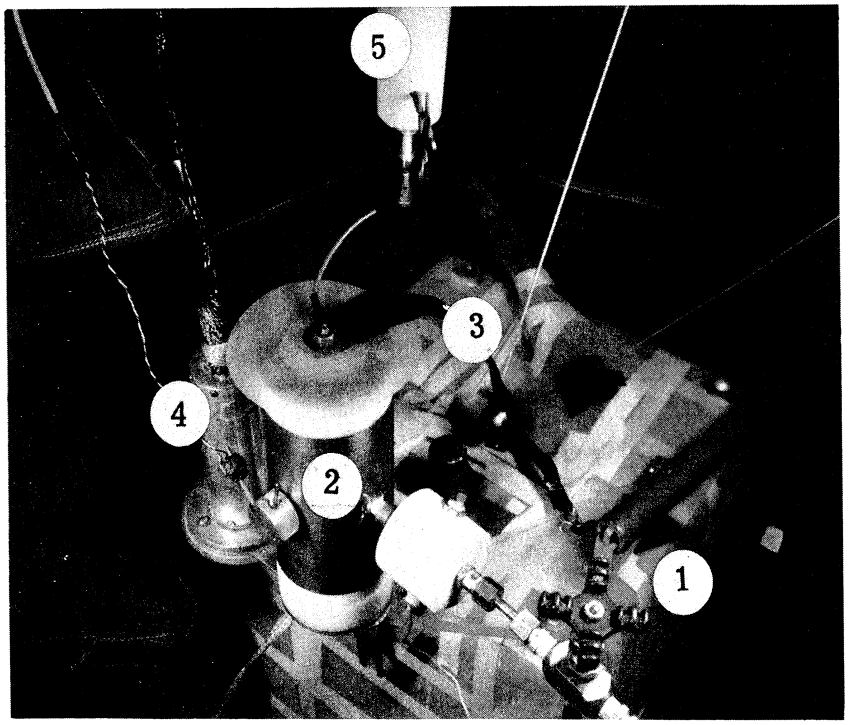

Figure B-1. The Exploding Wire System which was used to Study Metal Condensation

1. Capacitors
2. Pressure Chamber
3. "Drop" Switch
4. Current Shunt
5. Voltage Probe

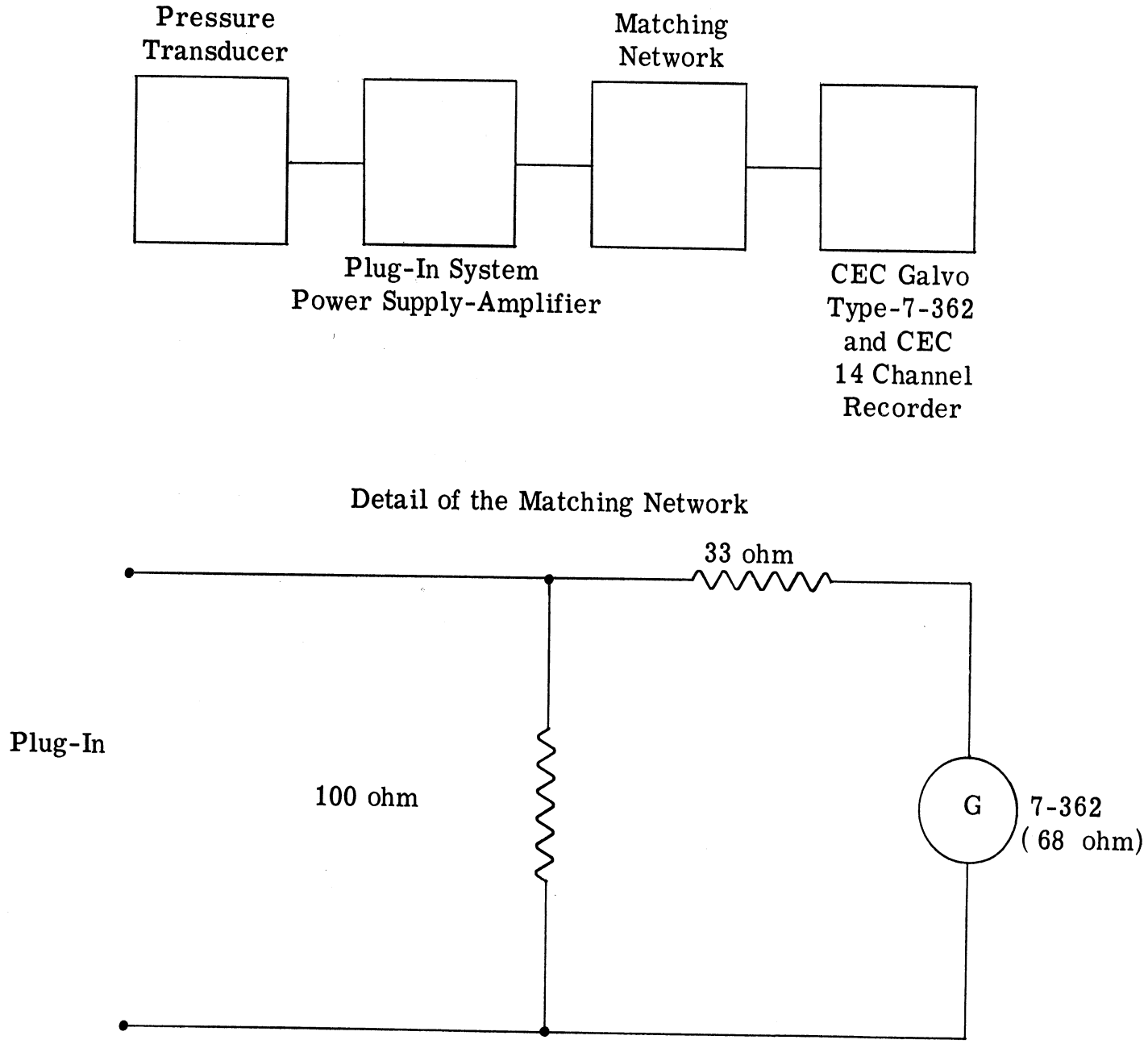

Figure B-2. Block Diagram of the Pressure Measurement System

APPENDIX C. SAMPLING APPARATUS AND TECHNIQUES

Vaporized zinc was introduced into the helium charged arc chamber by means of a zinc fuse and zinc center electrode. By measuring the weight of the fuse and electrode before and after a run, an upper limit to the amount of zinc vapor added to the helium was determined. This zinc vapor mass fraction varied on all tests between a value of 0. 4 and 0. 7 with the average value around 0. 6.

After the expansion of the zinc vapor and helium through a 15^{o} divergent nozzle the flow was "sampled" for zinc particles. The zinc particles collected on a carbon coated film were shadowed with chromium vapor and then photographed in an electron microscope. Figure C-1 shows an example of these photomicrographs. The particles were then counted and classified by size and the results plotted in the form of a size distribution curve. The percentage of particles lying within any size range is simply the integral of the curve over that range.

Due to the large amount of zinc in the flow, the particles had to be collected over a very short period of time and spread over a large area to enable analysis by means of an electron microscope. To accomplish this, a rotating cylinder collector was used in conjunction with a shutter arrangement.

Two different types of shutters were used: a rotating shutter and a solenoid actuated linear shutter. In both the principle was quite similar to the focal plane shutter used in a camera.

Rotating Shutter

Figure C-2 is a schematic of this sampling apparatus. Two concentric cylinders—a hollow exterior "shutter" cylinder with two opposite openings extending the full axial length, and a solid interior "collector" cylinder with attached sampling tape—were driven through a gear arrangement by a 12 volt d-c motor. The gear sizes were selected to give a collector speed of 5 1/4 times that of the shutter. In this way the deposits of zinc on the inner cylinder are spaced 225^{o} apart allowing eight spaced deposits before there is any overlap (see Fig. C-3). Since the shutter rotates at approximately 3000 rpm, this allows 80 msec of run time before overlapping occurs. The arc chamber dump port opens at 30 msec, so by 80 msec the chamber pressure has dropped to a very low level.

One of the major advantages of the rotating shutter lies in the fact that it allows a sampling across the entire width of the jet. The other basic advantage is that it collects particles at several distinct times during the run and therefore at different stagnation conditions.

The main disadvantage of this shutter lay in its inability to stop collection after 80 msec. Even though, as previously mentioned, the stagnation pressure was substantially lower (i. e. approximately 40 psia), it could still have been sufficient to "blow" dust from inside the chamber onto the collection cylinder. This seems to be substantiated by a large amount of "dirt" seen on the centerline where a subsonic stream would deposit. For this reason a linear "single shot" shutter was substituted for the rotating shutter.

Linear Shutter

Figure C-4 shows a schematic of the experimental arrangement used with this shuttering technique.

An aluminum shutter moves vertically in a triangular shaped housing. Both the shutter and the housing have openings in them which when aligned allow the flow to pass through and impinge on the collector cylinder.

The propelling device used for the shutter is a 6 volt d-c solenoid. The arc voltage trace is used as a time reference by employing this voltage (obtained from a small coil placed inside the hot-shot main power coil) as trigger input to a single beam, dual time base Tektronix Oscilloscope, Model 545A. The scope then puts out two gate signals; one (gate B) is concurrent with the input voltage and the other (gate A) can be delayed any desired amount. This latter voltage is used as input to a simple silicon-conctrolled-rectifier circuit (see Fig. C-5) which switches the power to the shutter solenoid. Since a 60 volt d-c source is used to drive the 6 volt, 1.5 ohm solenoid, the power needs to be shut off very quickly to eliminate a solenoid burn-out. This is accomplished by fusing the main circuit with a 5 ampere slow-blow fuse.

This shutter has the advantage of providing a definite known time of sampling with no extraneous particles. The time is determined accurately by means of a light beam shining through a small hole drilled through the triangular section. This hole is placed so that the shutter breaks the light beam at the same instant

the sample is taken. Thus a small light sensitive voltaic cell measuring the light beam gives a definite marking on the oscillograph record of the time of collection.

The two basic disadvantages of this shutter are: (1) only one collection is made during each run and (2) only 1/4 in. (the length of the opening in the shutter housing) of the flow is sampled (i. e. these eliminate a location-resolved, time-resolved sampling of the beam and result in only one point of information in time and location for each run).

The entrance slit in the housing was large compared to the radius of curvature of the razor blades used as beam splitters. Figure C-6 shows a photomicrograph of a cross section of the razor blade. It can be seen that the radius of curvature of the edge is less than 2.4×10^{-5} in., which when compared to the minimum slit opening used (6×10^{-3} in.) is small enough to be considered perfectly sharp.

However, another problem involving the slit width did arise. The razor blades were flexible enough to be deformed by the pressure differences arising during the run. Due to this phenomenon, the preset slit width was not the width encountered during the run. This created problems in adjustment of the blades to give desired tape deposit densities. The problem was somewhat alleviated by the addition of backup chisel-type blades (see Fig. C-7).

Figures C-8 and C-9 show a mica tape just after a hot-shot (run of 29 July 66). In Fig. C-8 the tape is still attached to the cylinder collector and

in Fig. C-9 it has been removed and labeled for electron microscope analysis. In this particular run the density of the collected zinc particles was too high to be analyzed in the dark region (it is generally found that if the deposit can be seen by the naked eye, it is too dense for analysis). However the pictures give an excellent example of the pattern left by the impinging zinc particles.

The sampler housing was enclosed when it was felt that zinc particles might be entering the sampler through the "side windows." However this enclosure would create a pressure difference after the run (the housing pressure being much less than the ambient receiver pressure in the vacuum tank). This pressure difference would create a flow through the various small openings in the housing, carrying the "zinc fog" (remaining suspended in the vacuum tank immediately following a run) into the housing. To eliminate this possibility a pressure line was run from the housing to atmosphere and blocked off by a magnetic valve. This valve was actuated by a silicon-controlled-rectifier circuit triggered by the B gate output of the scope mentioned above. As the response time of the magnetic valve was approximately 40 msec, the pressure in the housing started to rise immediately following the run. This would create a reverse flow, if anything, out of the small openings and prevent the contamination of the sampler interior.

Development Summary

Many problems arose during the development of the sampling apparatus to its present state. A brief summary is given here.

Electron microscope grids for particle collection were originally used but abandoned due to warpage from the initial carbon film coating. It was found that bioden tape proved to become too coarse during the run to allow subsequent examination of particles of less than 200 Å. When mica tape proved too bulky and stiff to use with the rotating shutter and the overlap mentioned above prevented any correlation between time and particle sample, the linear shutter was substituted for the rotating shutter. The collector cylinder still had to be rotated extremely fast and the razor blade beam splitter width set accurately to prevent too dense a collection. The setting of the slit width proved to be a major problem due to the pressure differences across the blades during the run. The final configuration used was with Gillette Super Stainless blades supported by smoothed X-Acto chisel blades and the slit width preset at .012 in. (see Fig. B-7).

Flow Pattern

When any type of measuring apparatus such as a sampler is placed in the flow, the question always arises as to whether the apparatus itself has a significant effect on the quantity being measured. For this reason the flow inside the sampler was analyzed in two different ways: (1) high speed schlieren movies of the beam were taken (see Ref. 5) and, (2) high speed movies were taken of tufts placed across the width of the housing. In both cases the results indicated that the beam remains relatively well defined after entering the sampler. As indicated in the above section, the razor blades are sharp

enough that the leading edge shock can be assumed to remain attached. Since the flow is shock free until impingement upon the rotating cylinder, the only external effect on the particles in the beam is due to the viscous mixing with the quiescent air inside the sampler housing. Since the ambient pressure inside the housing is matched to the static pressure of the flow, these effects are not considered great enough to raise the zinc to its vaporization temperature.

Zn Mass Flow Comparison

In the run of 11 Apr 66, it is assumed that all the zinc lost from the electrode tip and the fuse is vaporized, then the mass fraction of zinc vapor in the chamber can be calculated as . 505. The total mass flow at the time the sample was taken is then calculated to be 40. 0 gm/sec. Of this, . 505 is zinc vapor so the mass flow of zinc vapor out of the chamber is 20. 2 gm Zn/sec.

From the count of the particles collected on the sampler, the collection density is found to be 2.24×10^{-9} gm Zn/mm^2. Assuming a collection area of 450 mm^2, which corresponds to the "well-defined" parallelogram observed on the runs of 15 Sep 66 and 21 Oct 66, the amount of zinc collected is calculated to be 10^{-6} gm. If it is assumed this is the only zinc entering the . 01 x . 25 in. slit during the time it was open (1 msec), the mass flow rate of zinc entering the sampler is 10^{-3} gm/sec. Dividing this by the ratio of the sampler entrance area to the nozzle exit area, a mass flow rate of zinc can be calculated as 3. 33 gm Zn/sec.

The discrepancy between the two values obtained, 3. 33 and 20. 2 gm Zn/ sec, can be attributed to many sources: all of the zinc lost from the fuse and electrode was not vaporized, the area of the nozzle exit was not the effective area through which the total amount of zinc could be assumed to be flowing, the zinc flow was not uniformly distributed, there was zinc distributed over a much larger area than the parallelogram used in the calculation, the collection efficiency was not 100%, and the particle count was not 100% accurate.

Electron Microscope Techniques

When the particles collected are too small to be seen under an optical microscope, an electron microscope must be employed. The instrument used was of the transmitted beam type where the beam must pass through the surface to be examined. At least part of the surface must then be transparent to the beam. As mentioned earlier, in the case of the examination of small particles, the collection must then be sparse.

The procedure now being employed is based on the use of mica strips as a supporting surface. The mica is cleaved along lattice surfaces so that it is microscopically smooth and very thin. It is placed in an evaporator where a layer of carbon ~ 160 $\mathring{A}$ thick is deposited on it by evaporation and surface condensation at very low pressure. Such a carbon film is transparent to the electron beam. A much thicker layer would be opaque, while, a much thinner layer would be structurally weak. The carbon coated mica is pasted to the collection cylinder in the sampler by means of tape with adhesive on both sides.

After particles are collected, the mica strip is placed back in the evaporator where the surface is "shadowed" by evaporation of a thin film of chromium deposited at an angle to the surface. The chromium is opaque to the electron beam so that the shadows created permit three-dimensional analysis of the particles photographed. The higher a particle stands above the collection surface, the longer will be the shadow.

Copper grids consisting of a 1/8 in. diameter ring with a copper gauze or mesh mounted on it provide the ultimate support for the film to be examined in the electron microscope. The film consisting of carbon layer plus particles plus chromium layer is removed from each piece of the mica, which has been cut to grid size, by floating it off the mica in water. As the film floats on the water a copper grid is placed under it and the specimen is ready to be placed in the microscope and photographed.

The above procedure was developed after several other approaches were first used. Instead of mica, a layer of Biodine, and earlier a layer of collodion, was used. These support surfaces had two disadvantages. They were difficult to remove from the carbon film, since it had to be removed by dissolving in an extractor. In addition, both of these backings yielded a rough background surface so that very small particles might not be detected.

When particle collections are too dense to be examined directly there are two ways of obtaining photomicrographs. One is the replica method where an imprint of the specimen surface is made with something like collodion poured

over it and allowed to dry and later shadowed. The other is ultrasonic dispersion of the particles in a mixture of collodion and solvent which are then randomly spread out—or "resampled" on an appropriate support surface. Both of these methods have been used with only limited success. In addition, rock salt split along lattice surfaces and polished in distilled water was used as a collection surface. It could easily be dissolved in water so that the underside of the collection could be examined by the replica method. This method only works when there is no chemical reaction with the salt impairing the microscopically smooth surface.

The use of the copper grids coated with carbon directly mounted on the sampler met with almost no success primarily because of the difficulty of keeping the grids glued to the sampler surface. The carbon films with no back support except the copper grid also tended to tear.

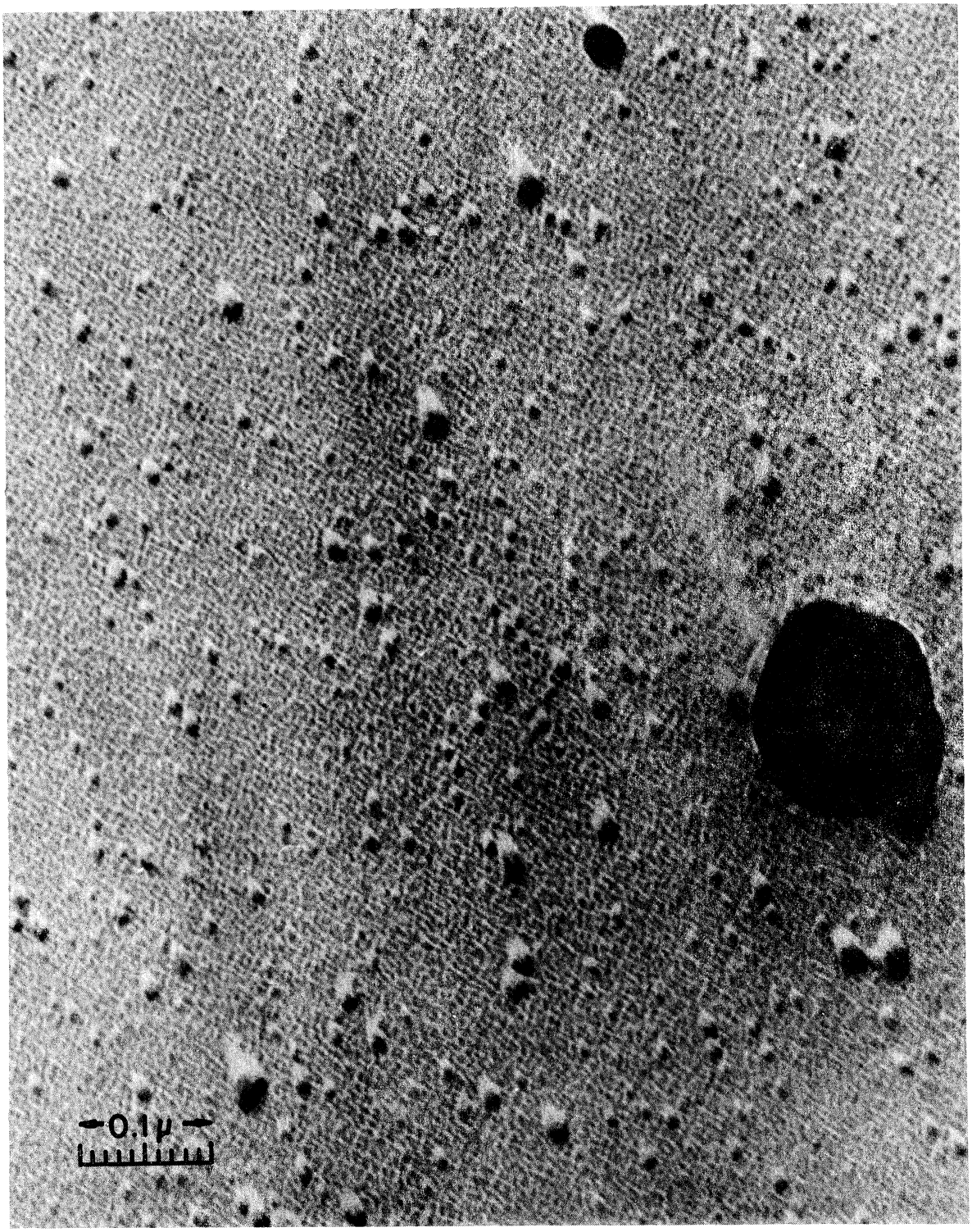

Figure C-1. Photomicrograph of Particles Collected in 11 Apr 66 Run. 216,000 X.

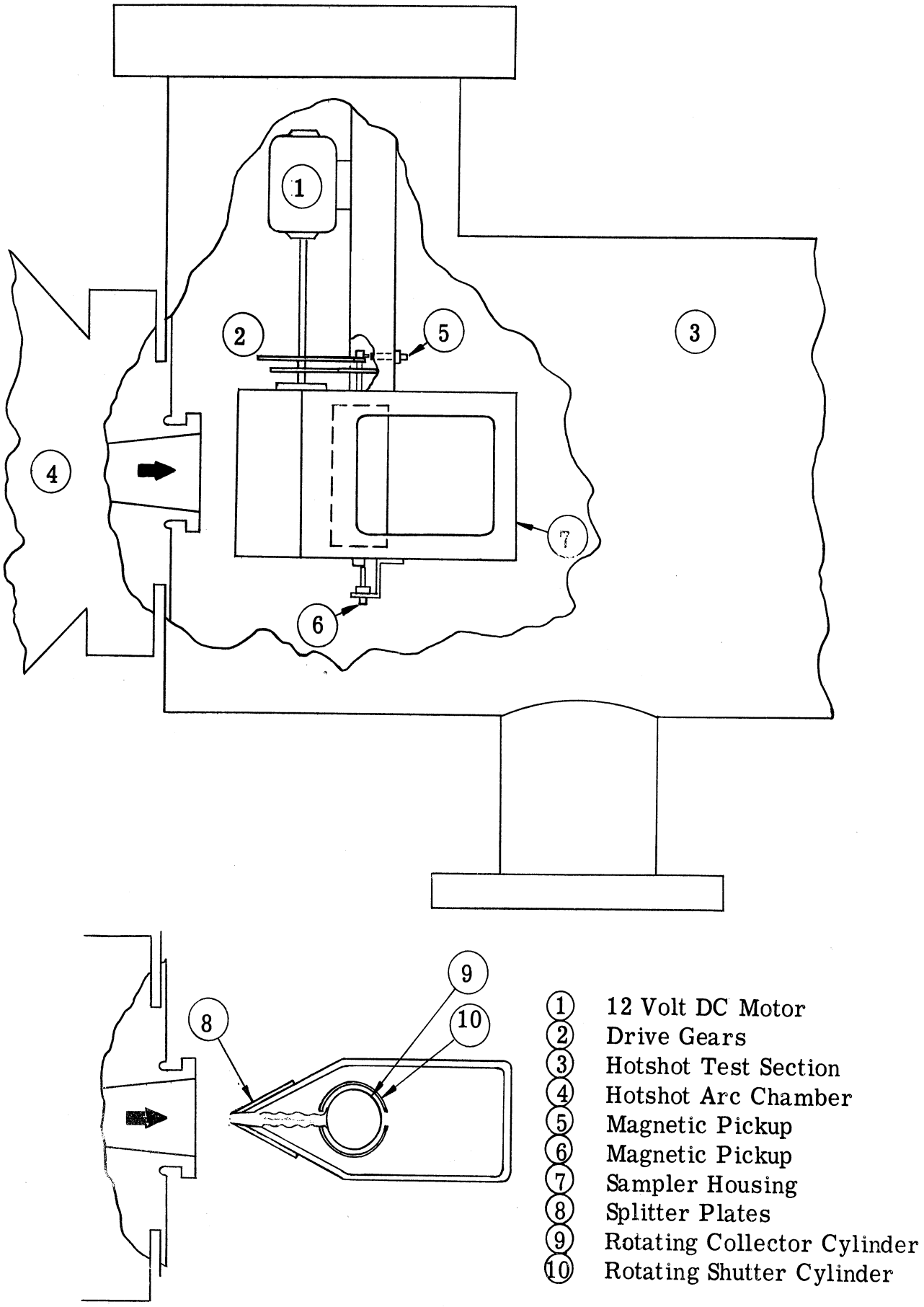

Figure C-2. Schematic of Rotating Shutter Sampling Apparatus Mounted in Hotshot Tunnel Test Section.

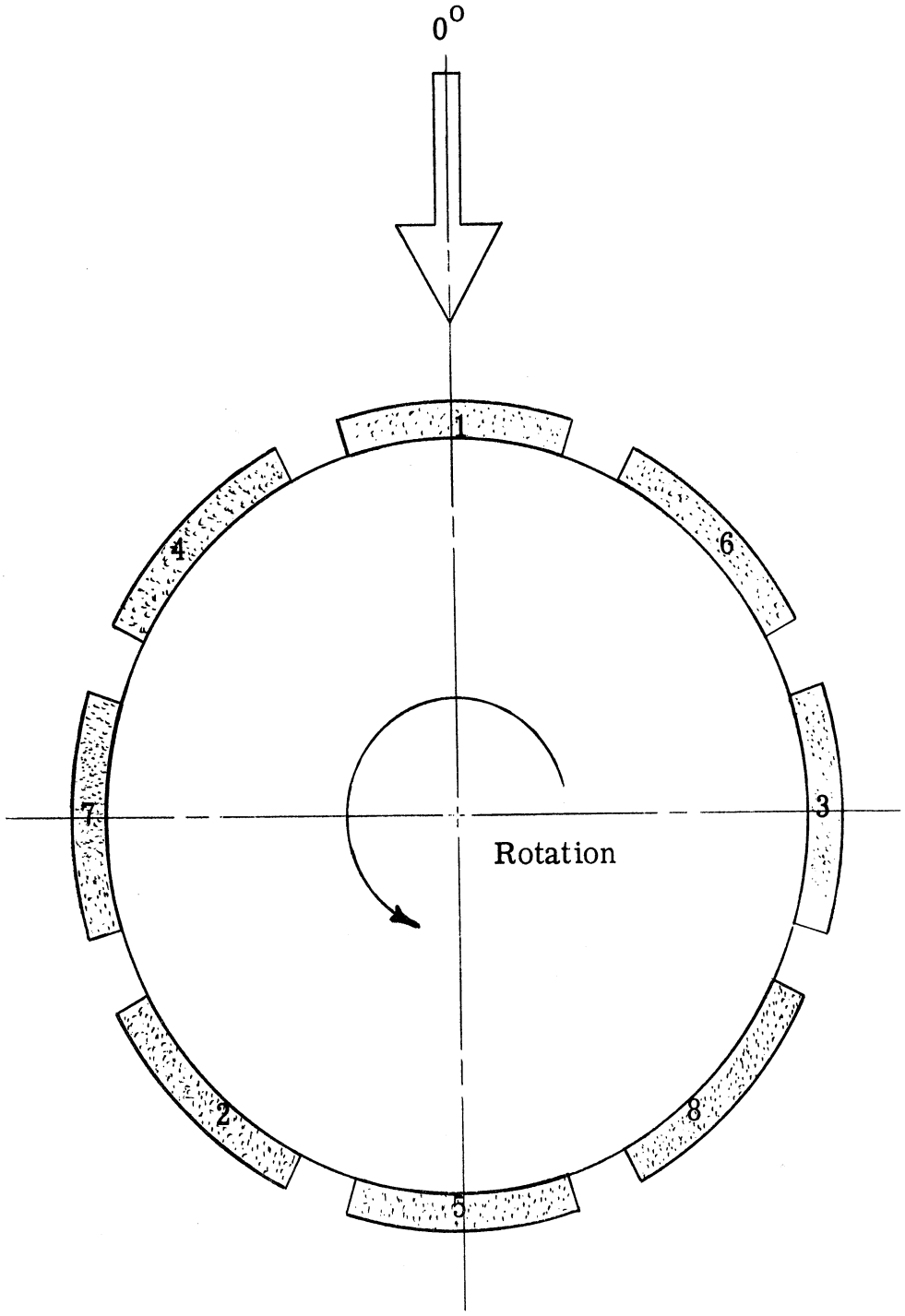

(Numbers indicate timewise order of sampling.)

Figure C-3. Collector Cylinder Sample Location Diagram (Rotating Shutter).

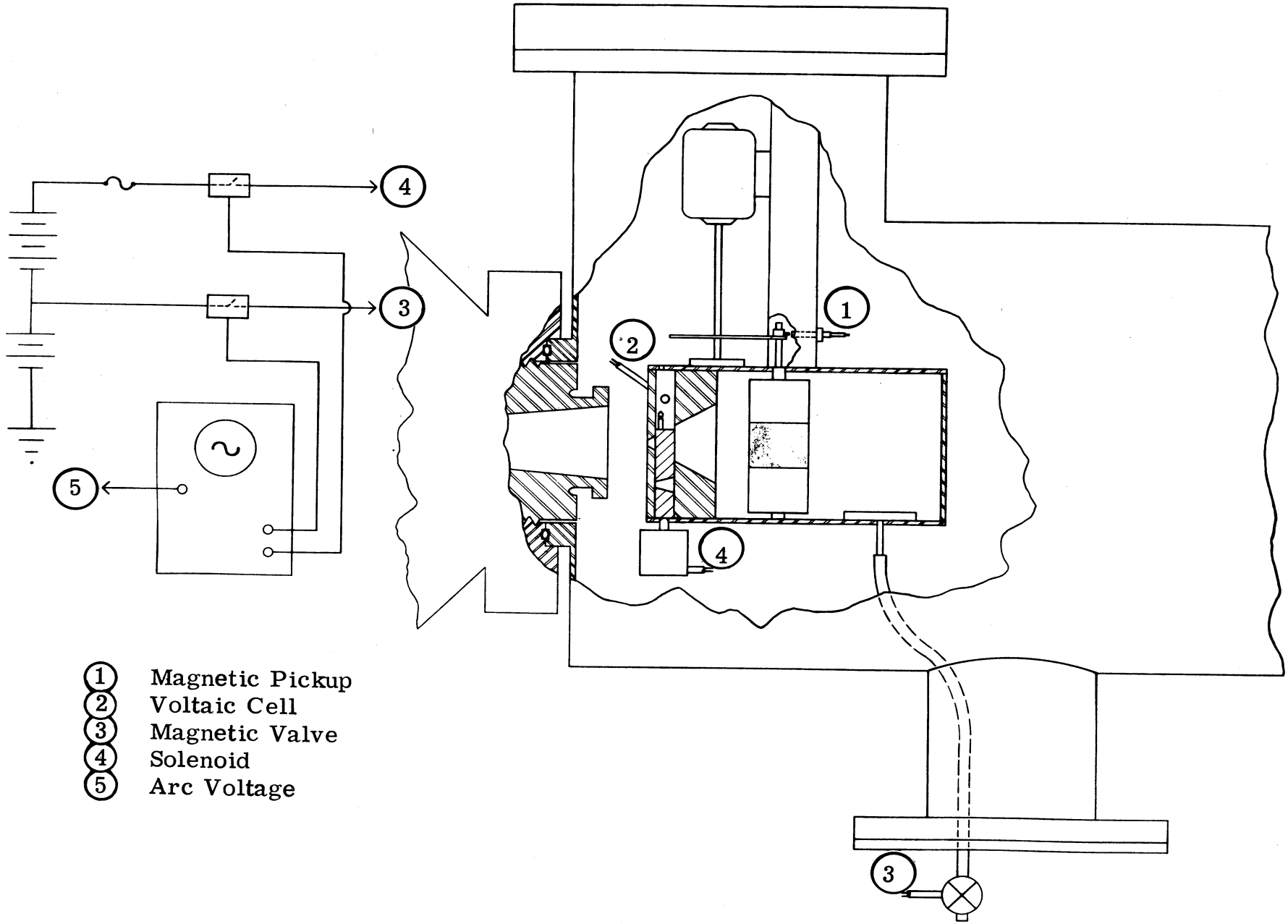

Figure C-4. Schematic of Linear Shutter Sampling Apparatus Mounted in Hotshot Tunnel Test Section.

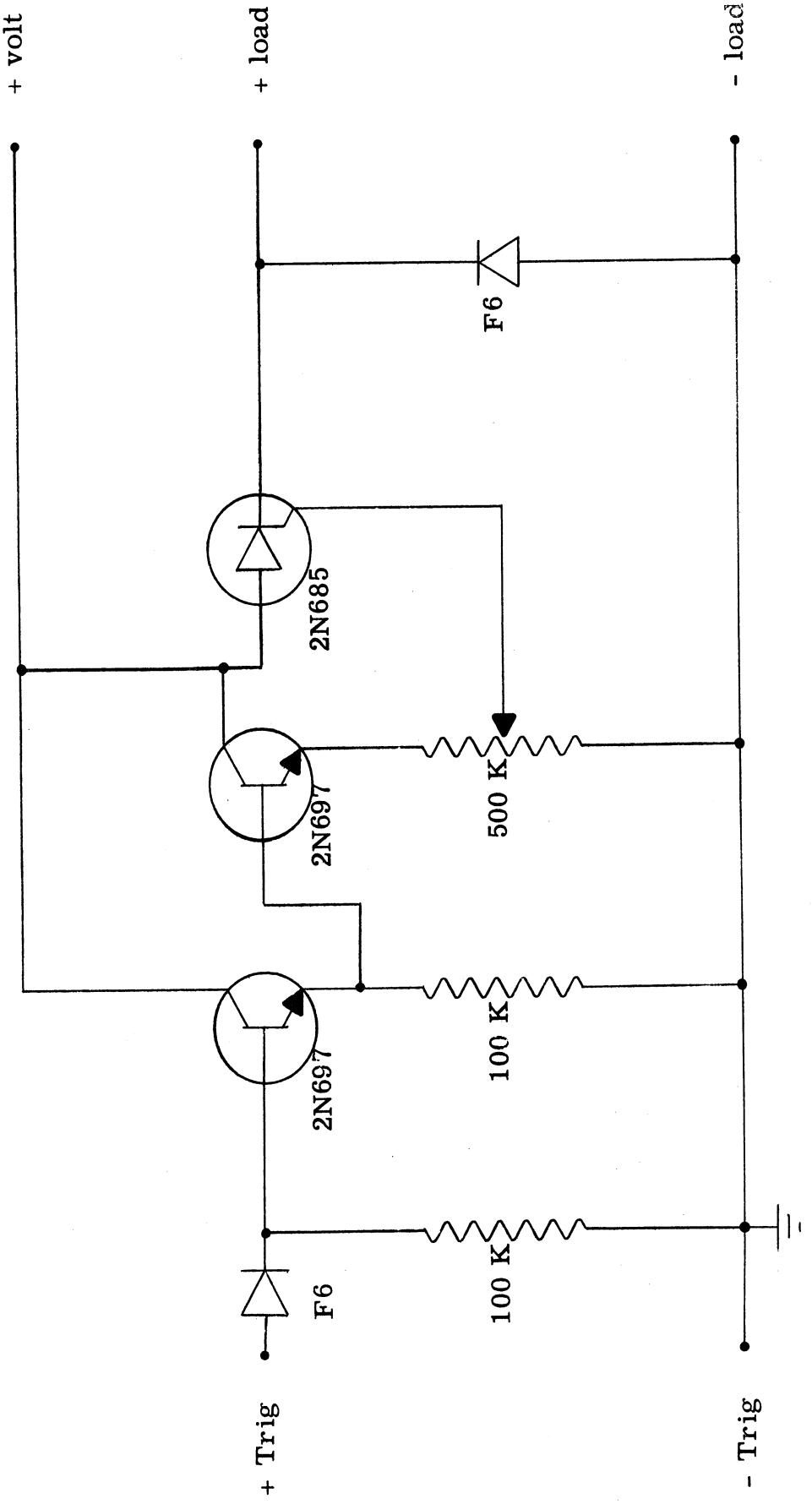

Figure C-5. Schematic of Silicon-Controlled-Rectifier Circuit.

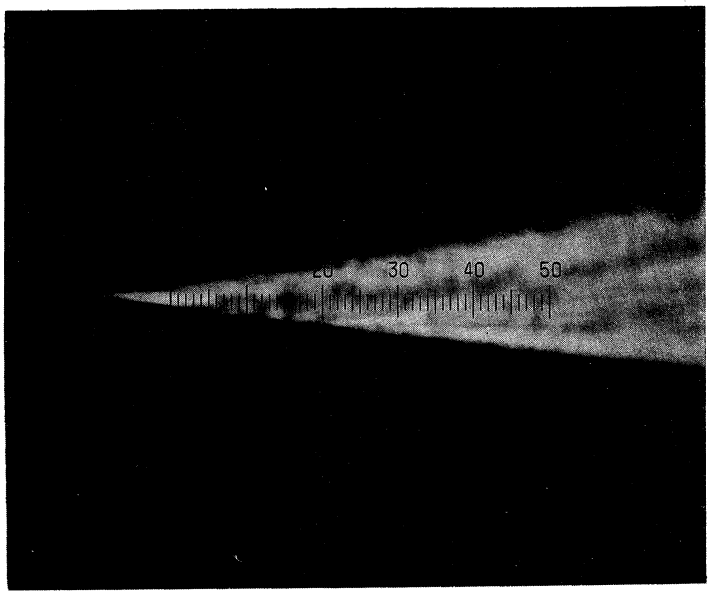

.05 mm

Figure C-6. Photomicrograph of Cross-Section of Gillette Super Stainless Razor Blade Edge. 875 X.

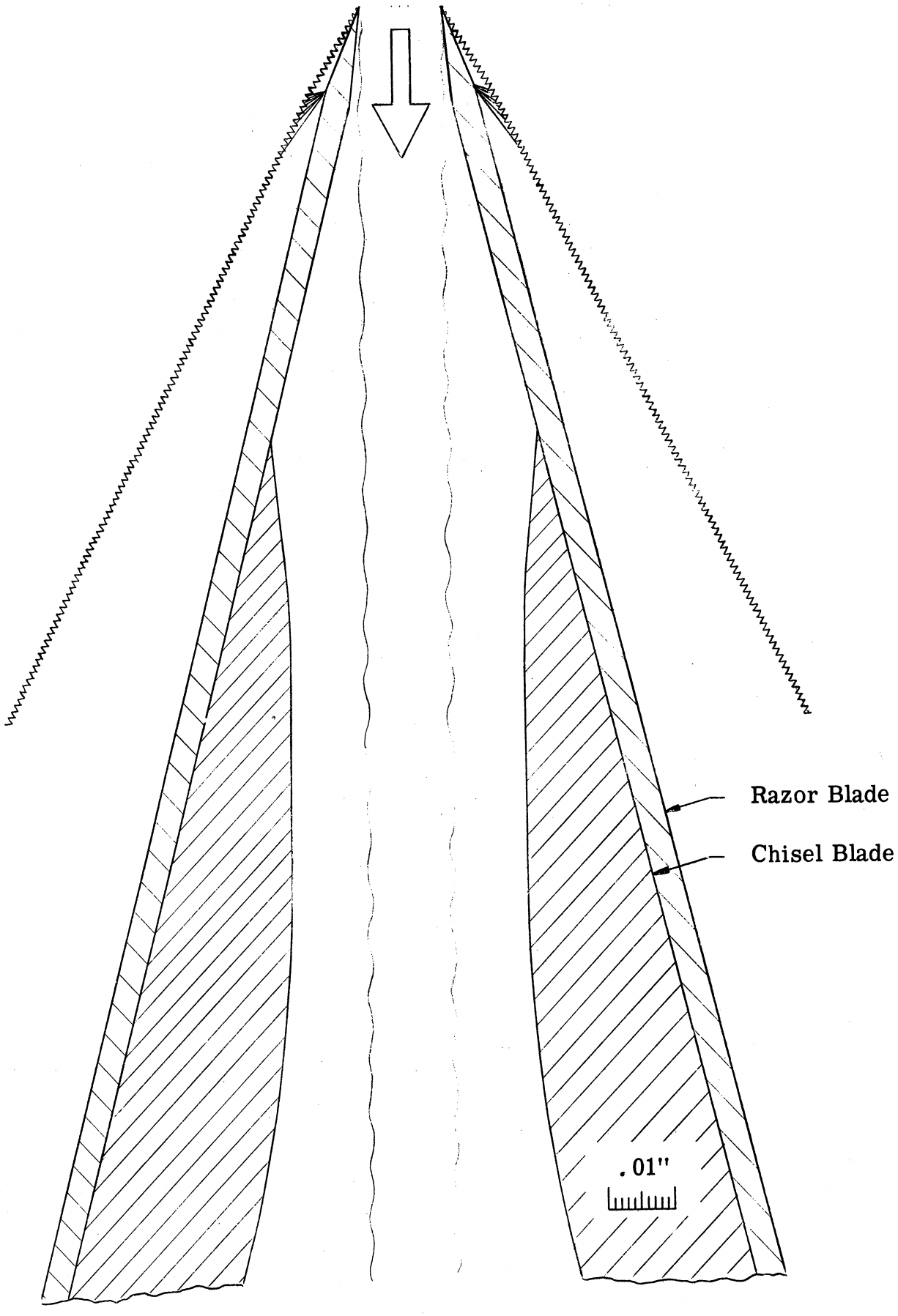

Figure C-7. Leading Edge Configuration for Linear Shutter Apparatus. 50 X.

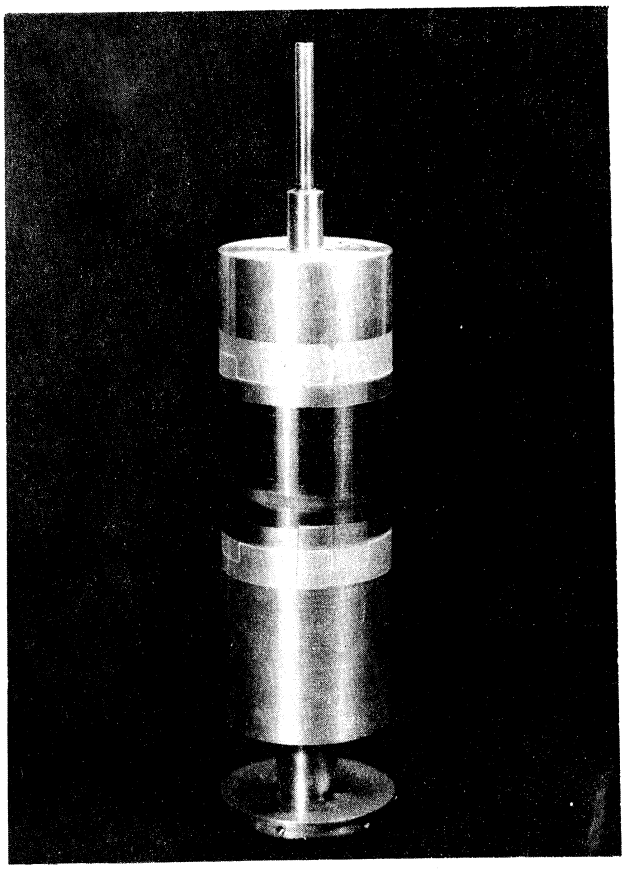

Figure C-8. Exposed Mica Tape on Collector Cylinder (following 29 Jul 66 run)

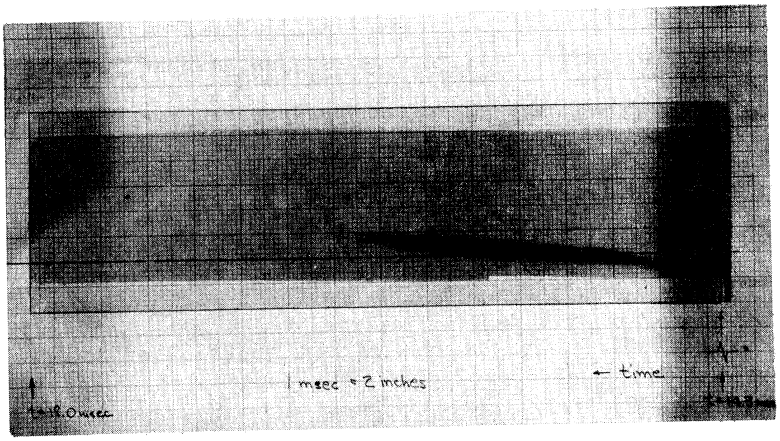

Figure C-9. Exposed Mica Tape Removed and Ready for Electron Microscope Analysis.

APPENDIX D. COMPUTER SOLUTIONS OF SIMPLIFIED CONDENSATION EQUATIONS

To obtain a reasonable estimate of the pressure rise that could be expected as a result of vapor condensing in an inert carrier medium, two simplified solutions of the condensation equations were made. The first solution was the "condensation shock" solution and the second was the "saturated equilibrium expansion" solution.

Figure D-1 shows both the saturated equilibrium solution and a locus of shock solutions compared with the isentropic expansion in the exploding wire nozzle. It can be seen that the "condensation shock" solution gives higher downstream pressures than does a saturated expansion solution, as mentioned in Ref. 2.

A list of the nomenclature used in this appendix is given here for convenience sake.

A	nozzle area
B	vapor pressure curve constant
C	vapor pressure curve constant
C_p	specific heat at constant pressure
g	ratio of density of condensed material to density of mixture
L	latent heat of vaporization of vapor
$\tilde{M}$	Mach number (defined in Eqs. D-2. 6)
p	pressure
R_o	universal gas constant
r^*	radius of nozzle throat
T	temperature

u	velocity
x	nozzle location
γ	ratio of specific heats
θ	half angle of nozzle
κ	ratio of density of condensible vapor to density of mixture
μ	molecular weight
ρ	density

Subscripts

1	upstream of "condensation shock"
2	downstream of "condensation shock"
v	condensible vapor
i	inert carrier gas
in	upstream of throat
out	downstream of throat
o	stagnation conditions

"Condensation Shock" Solution

The "condensation shock" solution is treated by Wegener and Mack for a one-component flow. The solution given here, while being similar in principle, is necessarily different in execution due to the fact that it is for a mixture of two gases, one condensible and one inert. This solution makes the following simplifying assumptions: (1) the flow is steady and one-dimensional, (2) the gaseous components are thermally and calorically perfect, (3) the flow is "frozen" isentropic to the "shock" location, (4) heat is added instantaneously at the "shock" discontinuity, and (5) the amount of heat added is just sufficient for the vapor to be in a saturated equilibrium state behind the "shock."

The governing equations are simply the common conservation equations at a discontinuity (with allowances made for the two-component mixture and the heat addition), the equation of state, and the Clausius-Clapyron equation (used to meet the requirement of saturation behind the shock).

(Mass) $$\rho_1 u_1 = \rho_2 u_2 \qquad \text{(D-1. 1)}$$

(Momentum) $$p_1 + \rho_1 u_1^2 = p_2 + \rho_2 u_2^2 \qquad \text{(D-1. 2)}$$

(Energy) $$C_{p_1} T_1 + \frac{u_1^2}{2} = C_{p_1} T_2 + \frac{u_2^2}{2} - Lg \qquad \text{(D-1. 3)}$$

(State) $$p_2 = (1 - g)\, \rho_2 R_2 T_2 \qquad \text{(D-1. 4)}$$

(Saturation) $$p_{2_v} = \exp\left(B - \frac{C}{T_2}\right) \qquad \text{(D-1. 5)}$$

(Note: in Eq. (D-1. 3), the C_{p_1} on the right side of the equation is used to account for the enthalpy of the condensed vapor (see Ref. 2, p. 369)).

The first four equations can be solved to give a quadratic expression in p_2. One solution corresponds to the normal shock with heat addition and is discarded. The other solution is for the heat addition only and is:

$$p_2 = \frac{-\beta + \sqrt{\beta^2 - 4\alpha\xi}}{2\alpha} \qquad \text{(D-1. 6)}$$

where:

$$\left.\begin{aligned}
\alpha &= -\frac{1}{2\rho_1^2 u_1^2}\left[\frac{2\gamma}{\gamma - 1}\frac{(1 - \kappa_o)\,\mu_v + \kappa_o\,\mu_i}{(1 - \kappa_o)\,\mu_v + (\kappa_o - g)\,\mu_i} - 1\right] \\
\beta &= \frac{p_1 + \rho_1 u_1^2}{\rho_1^2 u_1^2}\left[\frac{\gamma}{\gamma - 1}\frac{(1 - \kappa_o)\,\mu_v + \kappa_o\,\mu_i}{(1 - \kappa_o)\,\mu_v + (\kappa_o - g)\,\mu_i} - 1\right] \\
\xi &= \frac{\left(p_1 + \rho_1 u_1^2\right)^2}{\rho_1^2 u_1^2} - C_{p_1} T_1 - \frac{u_1^2}{2} - Lg
\end{aligned}\right\} \quad \text{(D-1. 7)}$$

T_2 can be obtained from a simultaneous solution of Eqs. (D-1. 1, 1. 2, 1. 3) to give:

$$T_2 = \frac{1}{C_{p_1}}\left\{-\xi + \frac{p_2}{2\rho_1^2 u_1^2}\left[2\left(p_1 + \rho_1 u_1^2\right) - p_2\right]\right\} \qquad \text{(D-1. 8)}$$

The ratio of partial vapor pressure to total pressure can be easily calculated to give:

$$\frac{p_{2_v}}{p_2} = \frac{(\kappa_o - g)\,\mu_i}{(1 - \kappa_o)\,\mu_v + (\kappa_o - g)\,\mu_i} \qquad \text{(D-1. 9)}$$

Due to the laboriousness of the calculations, the above equations were programmed for solution on the IBM 7090 digital computer. Equations (D-1. 6, 1. 7, 1. 8, and 1. 9) were solved on the computer for p_{2_v} for incremental jumps of g until a solution was reached which agreed with p_{2_v} as given by a simultaneous solution of Eq. (D-1. 5).

This procedure was followed for incremental steps in nozzle location to give a locus of pressures downstream of the condensation as a function of nozzle location. These values are somewhat higher than a condensing stream would yield but nonetheless serve to give a good estimate.

Saturated Equilibrium Expansion

Wegener and Mack derive the one-dimensional condensation equations for a two-component mixture of a condensible vapor in an inert carrier gas. The simplifying assumptions are: (1) the condensed mass is uniformly distributed throughout the expanding vapor-carrier mixture, (2) the condensed mass has the same velocity and temperature as the mixture, (3) the gaseous components are assumed thermally and calorically perfect, (4) the flow is considered to be steady and one-dimensional, and (5) the density of the liquid phase is much greater than the density of the vapor phase allowing neglect of its volume. The equations for the flow of a condensible vapor and inert carrier gas in equilibrium with the condensed phase are the conservation equations of mass, momentum, and energy, the equation of state, and the Clausius-Clapyron equation (specifying the vapor pressure curve for the condensible vapor). These equations in their differential form are:

(Mass)
$$\frac{d\rho}{\rho} + \frac{du}{u} + \frac{dA}{A} = 0 \qquad \text{(D-2. 1)}$$

(Momentum)
$$\frac{dp}{p} + \frac{\gamma \tilde{M}^2}{1 - g} \frac{du}{u} = 0 \qquad \text{(D-2. 2)}$$

(Energy)
$$(\gamma - 1)\,\tilde{M}^2 \frac{du}{u} + \frac{C_{p_o}}{C_p}\frac{dT}{T} - \frac{L}{C_p T}\,dg = 0 \qquad \text{(D-2. 3)}$$

(State)
$$\frac{dp}{p} - \frac{d\rho}{\rho} - \frac{dT}{T} + \frac{\mu}{\mu_v}\frac{dg}{1 - g} = 0 \qquad \text{(D-2. 4)}$$

(Vapor Pressure)
$$\frac{dp_v}{p_v} - \frac{\gamma}{\gamma - 1}\frac{L}{C_{p_v} T}\frac{dT}{T} = 0 \qquad \text{(D-2. 5)}$$

where:

$$\left.\begin{aligned}
\tilde{M} &\equiv \frac{u}{\sqrt{\gamma \dfrac{R_o}{\mu} T}} \\
C_p &= \frac{1}{1 - g}\left[(1 - \kappa_o)\, C_{p_i} + (\kappa_o - g)\, C_{p_v}\right] \\
\mu &= \frac{(1 - g)\,\mu_i\,\mu_v}{(1 - \kappa_o)\,\mu_v + (\kappa_o - g)\,\mu_i} \\
\gamma &\equiv \frac{C_p}{C_p - R_o/\mu} \\
p_v &= \frac{(\kappa_o - g)\,\mu_i}{(1 - \kappa_o)\,\mu_v + (\kappa_o - g)\,\mu_i}\, p
\end{aligned}\right\} \qquad \text{(D-2. 6)}$$

Equation (D-2. 5) can be combined with the last of Eqs. (D-2. 6) to give a revised vapor pressure equation:

$$\frac{dg}{1 - g} - \frac{(\kappa_o - g)}{(1 - g)}\left\{\frac{C_{p_o}\,\mu_i\, T - L\left[(1 - \kappa_o)\,\mu_v + (\kappa_o - g)\,\mu_i\right]}{(1 - \kappa_o)\, R_o T + (\kappa_o - g)\, L\,\mu_i}\right\}\frac{dT}{T} = 0 \qquad \text{(D-2. 7)}$$

The geometry of a conical nozzle with axial distance, x, equal to zero at the throat, yields the differential equation,

$$\left.\begin{aligned} \frac{dx}{x} - \frac{r^* - x \tan \theta_{in}}{-2x \tan \theta_{in}} \frac{dA}{A} = 0, \qquad x < 0 \\ \frac{dx}{x} - \frac{r^* + x \tan \theta_{out}}{2x \tan \theta_{out}} \frac{dA}{A} = 0, \qquad x > 0 \end{aligned}\right\} \qquad \text{(D-2. 8)}$$

Equations (D-2. 1, 2. 2, 2. 3, 2. 4, 2. 7, and 2. 8, were reduced to the form:

$$\left.\begin{aligned} \frac{dp}{dx} &= f_1 (p, \rho, u, T, g, A, x) \\ \frac{d\rho}{dx} &= f_2 (p, \rho, u, T, g, A, x) \\ \frac{du}{dx} &= f_3 (p, \rho, u, T, g, A, x) \\ \frac{dT}{dx} &= f_4 (p, \rho, u, T, g, A, x) \\ \frac{dg}{dx} &= f_5 (p, \rho, u, T, g, A, x) \\ \frac{dA}{dx} &= f_6 (p, \rho, u, T, g, A, x) \end{aligned}\right\} \qquad \text{(D-2. 9)}$$

where:

$$f_1 = \frac{p}{X_8} (X_1 X_3 - X_1 X_4 X_6)$$

$$f_2 = \frac{\rho}{X_8} (X_3 - X_4 X_6 - X_8)$$

$$f_3 = \frac{u}{X_8} (X_4 X_6 - X_3)$$

$$f_4 = \frac{T}{X_8}(X_2)$$

$$f_5 = \frac{1 - g}{X_8}(X_2X_6)$$

$$f_6 = \frac{A}{X_7}$$

$$X_1 = \frac{\gamma \tilde{M}^2}{1 - g}$$

$$X_2 = (\gamma - 1)\,\tilde{M}^2$$

$$X_3 = \frac{C_{p_o}}{C_p}$$

$$X_4 = \frac{L\,(1 - g)}{C_p T}$$

$$X_5 = \frac{\mu}{\mu_v}$$

$$X_6 = \frac{(\kappa_o - g)}{(1 - g)} \frac{C_{p_o}\,\mu_i\,T - L\left[(1 - \kappa_o)\,\mu_v + (\kappa_o - g)\,\mu_i\right]}{(1 - \kappa_o)\,R_o T + L\,\mu_i\,(\kappa_o - g)}$$

$$X_7 = \begin{cases} \dfrac{r^* - x \tan \theta_{in}}{-2x \tan \theta_{in}} & (x < 0) \\ \dfrac{r^* + x \tan \theta_{out}}{2x \tan \theta_{out}} & (x > 0) \end{cases}$$

$$X_8 = X_7\,(X_2 - X_2X_5X_6 + X_3 - X_4X_6 - X_1X_3 + X_1X_4X_6)\,x$$

Equations D-2. 9 form a set of six ordinary non-linear differential equations that were programmed for simultaneous solution on the IBM 7090 digital computer. The solution was obtained by means of a Runge-Kutta method stepwise integration with initial conditions furnished at the saturation point.

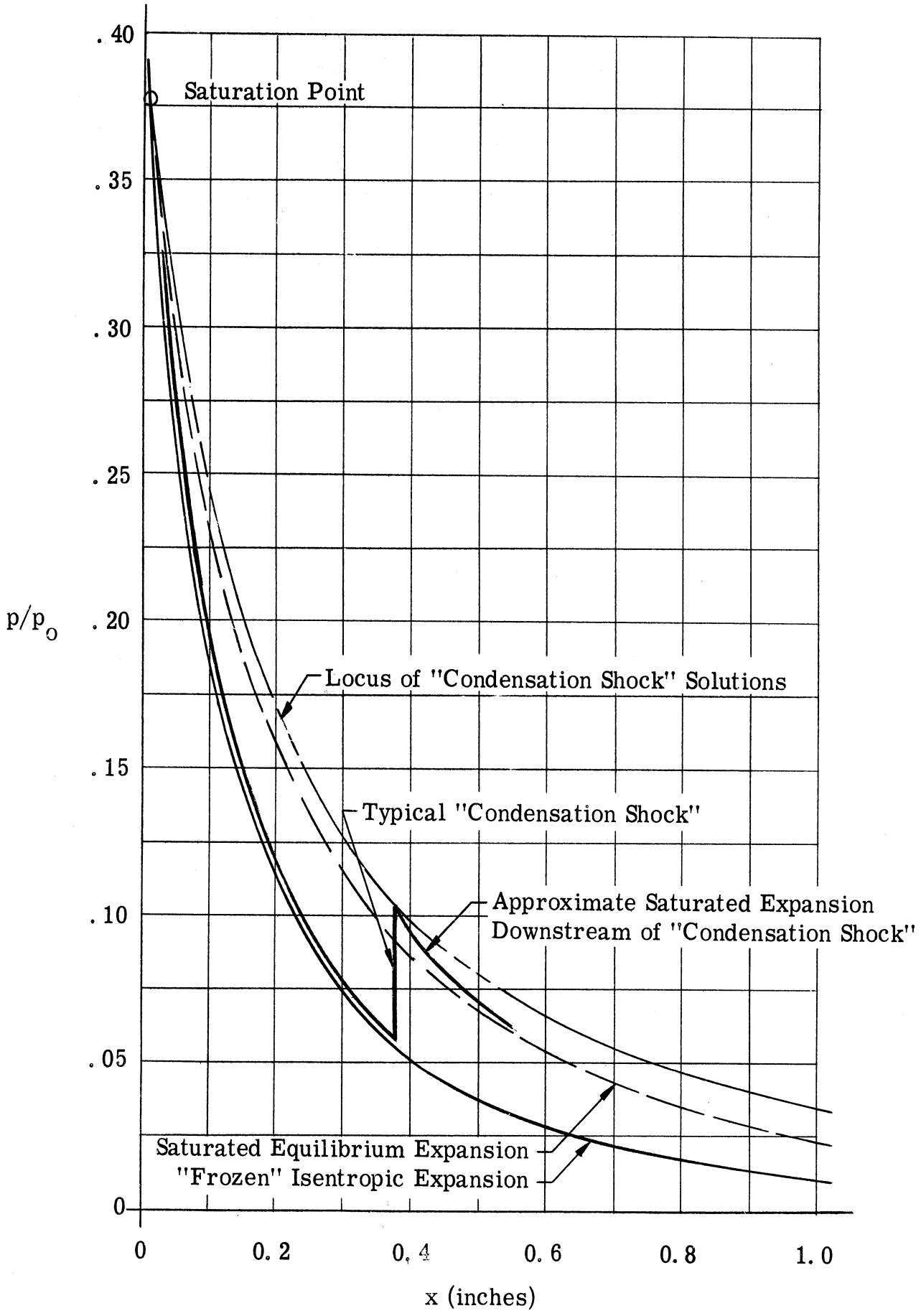

Figure D-1. Computed Solutions of Simplified Condensation Equations for the Mach 3 Nozzle (p_o = 590 psia, T_o = 1799^{o}K, κ_o = . 625)

APPENDIX E. DERIVATION OF THE ENERGY BALANCE EQUATION FOR EXPLODING WIRE ZINC IN HELIUM EXPERIMENTS

It is first assumed that all of the stored energy of the capacitor, E, is available to vaporize the wire, and heat the gas-vapor mixture to a final temperature T_f. Of this energy ΔE_{Zn} goes into vaporizing the wire and raising the temperature of the zinc vapor to T_f, and ΔE_{He} goes into raising the temperature of the helium gas from room temperature to T_f.

$$E = \Delta E_{Zn} + \Delta E_{He} \tag{E-1}$$

$$\begin{aligned} \Delta E_{Zn} &= m_{Zn}\, \Delta e_{Zn} \\ \Delta E_{He} &= m_{He}\, \Delta e_{He} \end{aligned} \tag{E-2}$$

$$\Delta e_{Zn} = (T_{mp} - T_{rt})\, C_{p_s} + \delta e_F + (T_v - T_{mp})\, C_{p_L} + \delta e_V + (T_f - T_v)\, C_{v_g} \tag{E-3}$$

$$\Delta e_{He} = (T_f - T_{rt})\, C_{v_{He}} \tag{E-4}$$

where

T_{rt} = Room temperature

= $298^{o}K$

T_{mp} = Melting point temperature of zinc

= $693^{o}K$

T_v = Vaporization temperature of zinc at atmospheric pressure

= $1181^{o}K$

T_f = Final temperature of mixture

C_{p_s} = Specific heat (at constant pressure) of zinc in solid phase

= .101 cal/gm^{o}K

C_{p_L} = Specific heat (at constant pressure) of zinc in liquid phase

= .115 cal/gm^{o}K

C_{v_g} = Specific heat (at constant volume) of zinc in vapor phase

= .046 cal/gm^{o}K

$C_{v_{He}}$ = Specific heat (at constant volume) of helium

= .754 cal/gm^{o}K

δe_F = Heat of fusion of zinc

= 24.2 cal/gm

δe_V = Heat of vaporization of zinc

= 425.6 cal/gm

m_{Zn} = Mass of zinc in grams

m_{He} = Mass of helium in grams

By substitution of (E-2, 3, 4) into Eq. (E-1),

$$E = (.754\ T_f - 225)\ m_{He} + (.046\ T_f + 491.5)\ m_{Zn} \qquad \text{(E-5)}$$

T_f may then be calculated for a given stored energy E. This temperature can then be compared with the calculation of temperature based on the measured stagnation pressure, assuming an ideal gas mixture to determine efficiency.

REFERENCES

1. Stever, H. G., "Condensation in High Speed Flows," High Speed Aerodynamics and Jet Propulsion, Vol. III, Princeton Univ. Press, 1958.

2. Wegener, P. P. and Mack, L. M., "Condensation in Supersonic and Hypersonic Wind Tunnels," Advances in Applied Mechanics, Vol. V, Academic Press, 1958.

3. Feder, Hirth, Courtney, et al., "Heterogeneous Combustion-Part iv-Condensation," Progress in Astronautics and Aeronautics, Vol. 15, Academic Press, 1964.

4. Sherman, P. M., "Development and Operation of an Arc Heated Hypersonic Tunnel," University of Michigan Report 02953-3-F, July 1963.

5. Sivier, K. R., Lu, P. L., McBride, D. D., and Oktay, E., "Initial Studies of Condensing Metal Vapors Carried by Expanding Inert Gases," ARL Report 65-59, March 1965.

6. Griffin, J. L. and Sherman, P. M., "Computer Analysis of Condensation in Highly Expanded Flows," AIAA Jour., October 1965.

7. Sivier, K. R., "Digital Computer Studies of Condensation in Expanding One-Component Flows," ARL Report 65-234, November 1965.

8. Thomann, H., "Determination of the Size of Ice Crystals Formed During Condensation of Water in Wind Tunnels and of their Effect on Boundary Layers," The Aeronautical Research Institute of Sweden, Report 101, July 1964.

Unclassified

Security Classification

DOCUMENT CONTROL DATA - R&D

(Security classification of title, body of abstract and indexing annotation must be entered when the overall report is classified)

1. ORIGINATING ACTIVITY *(Corporate author)*
The University of Michigan
Department of Aerospace Engineering
Ann Arbor, Michigan 48105

2a. REPORT SECURITY CLASSIFICATION
Unclassified

2b. GROUP

3. REPORT TITLE

Condensation in a Rapidly Expanding Metal Vapor-Inert Gas Mixture

4. DESCRIPTIVE NOTES *(Type of report and inclusive dates)*
Scientific. Final.

5. AUTHOR(S) *(Last name, first name, initial)*
Sherman, P.M., McBride, D.D., Oktay, E.

6. REPORT DATE	7a. TOTAL NO. OF PAGES	7b. NO. OF REFS
April 1967	88	8

8a. CONTRACT OR GRANT NO.	9a. ORIGINATOR'S REPORT NUMBER(S)
AF33(615)-2307	
b. PROJECT NO. 7116	
c. DoD Element 61445014	9b. OTHER REPORT NO(S) *(Any other numbers that may be assigned this report)*
d. DoD Subelement 681308	ARL 67-0071

10. AVAILABILITY/LIMITATION NOTICES

1. This document has been approved for public release and sale; its distribution is unlimited.

11. SUPPLEMENTARY NOTES	12. SPONSORING MILITARY ACTIVITY
TECH OTHER	Aerospace Research Laboratories (ARE) Wright-Patterson AFB, Ohio 45433

13. ABSTRACT

An investigation of the condensation of metal vapor in an inert carrier gas accelerated through nozzles is being carried out. The mixture used is primarily zinc vapor in helium gas. The zinc vapor is produced in two separate experimental arrangements. One is in the arc chamber of an inductance type hot shot tunnel. The other is in an exploding-wire chamber with a capacitor energy storage. Two types of condensation measurements are made. Measurement of particle size is made in the tunnel. Determination of condensation onset point is made in the exploding-wire system. Particle size is determined by means of a shuttered sampling device developed for the purpose combined with electron microscope techniques evolved. The condensation onset point is determined by nozzle static pressure measurement. Simplified computational analyses are made to predict conditions for the measured condensation onset point. They are also used as a guide for the more complex two component non-equilibrium expansion computation which may predict the location of the onset point as well as particle size. Measurements of particle size at the exit of a nominal Mach 25 (helium) nozzle showed a major portion of the total particles to less than ~70 Å in diameter. The pressure measurements made in a nominal Mach 3 nozzle indicated a large degree of supercooling. Further studies and evaluations to be made are discussed.

DD FORM 1 JAN 64 1473

Unclassified

Security Classification

14. KEY WORDS	LINK A		LINK B		LINK C	
	ROLE	WT	ROLE	WT	ROLE	WT
Metal Vapors Condensation Microscopic Particles Electron Microscope Two Component Flow Particle Size Measurement						

INSTRUCTIONS

1. ORIGINATING ACTIVITY: Enter the name and address of the contractor, subcontractor, grantee, Department of Defense activity or other organization *(corporate author)* issuing the report.

2*a*. REPORT SECURITY CLASSIFICATION: Enter the overall security classification of the report. Indicate whether "Restricted Data" is included. Marking is to be in accordance with appropriate security regulations.

2*b*. GROUP: Automatic downgrading is specified in DoD Directive 5200.10 and Armed Forces Industrial Manual. Enter the group number. Also, when applicable, show that optional markings have been used for Group 3 and Group 4 as authorized.

3. REPORT TITLE: Enter the complete report title in all capital letters. Titles in all cases should be unclassified. If a meaningful title cannot be selected without classification, show title classification in all capitals in parenthesis immediately following the title.

4. DESCRIPTIVE NOTES: If appropriate, enter the type of report, e.g., interim, progress, summary, annual, or final. Give the inclusive dates when a specific reporting period is covered.

5. AUTHOR(S): Enter the name(s) of author(s) as shown on or in the report. Enter last name, first name, middle initial. If military, show rank and branch of service. The name of the principal author is an absolute minimum requirement.

6. REPORT DATE: Enter the date of the report as day, month, year; or month, year. If more than one date appears on the report, use date of publication.

7*a*. TOTAL NUMBER OF PAGES: The total page count should follow normal pagination procedures, i.e., enter the number of pages containing information.

7*b*. NUMBER OF REFERENCES: Enter the total number of references cited in the report.

8*a*. CONTRACT OR GRANT NUMBER: If appropriate, enter the applicable number of the contract or grant under which the report was written.

8*b*, 8*c*, & 8*d*. PROJECT NUMBER: Enter the appropriate military department identification, such as project number, subproject number, system numbers, task number, etc.

9*a*. ORIGINATOR'S REPORT NUMBER(S): Enter the official report number by which the document will be identified and controlled by the originating activity. This number must be unique to this report.

9*b*. OTHER REPORT NUMBER(S): If the report has been assigned any other report numbers *(either by the originator or by the sponsor)*, also enter this number(s).

10. AVAILABILITY/LIMITATION NOTICES: Enter any limitations on further dissemination of the report, other than those imposed by security classification, using standard statements such as:

(1) "Qualified requesters may obtain copies of this report from DDC."

(2) "Foreign announcement and dissemination of this report by DDC is not authorized."

(3) "U. S. Government agencies may obtain copies of this report directly from DDC. Other qualified DDC users shall request through

_____."

(4) "U. S. military agencies may obtain copies of this report directly from DDC. Other qualified users shall request through

_____."

(5) "All distribution of this report is controlled. Qualified DDC users shall request through

_____."

If the report has been furnished to the Office of Technical Services, Department of Commerce, for sale to the public, indicate this fact and enter the price, if known.

11. SUPPLEMENTARY NOTES: Use for additional explanatory notes.

12. SPONSORING MILITARY ACTIVITY: Enter the name of the departmental project office or laboratory sponsoring *(paying for)* the research and development. Include address.

13. ABSTRACT: Enter an abstract giving a brief and factual summary of the document indicative of the report, even though it may also appear elsewhere in the body of the technical report. If additional space is required, a continuation sheet shall be attached.

It is highly desirable that the abstract of classified reports be unclassified. Each paragraph of the abstract shall end with an indication of the military security classification of the information in the paragraph, represented as *(TS)*, *(S)*, *(C)*, *or (U)*.

There is no limitation on the length of the abstract. However, the suggested length is from 150 to 225 words.

14. KEY WORDS: Key words are technically meaningful terms or short phrases that characterize a report and may be used as index entries for cataloging the report. Key words must be selected so that no security classification is required. Identifiers, such as equipment model designation, trade name, military project code name, geographic location, may be used as key words but will be followed by an indication of technical context. The assignment of links, rules, and weights is optional.